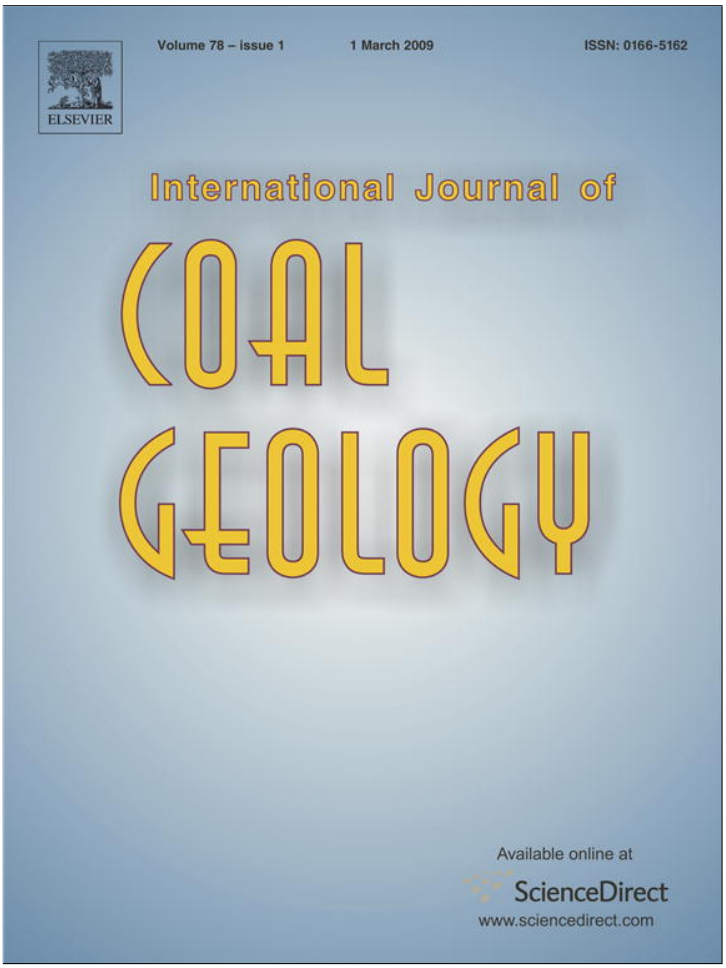

International Journal of Coal Geology 78 (2009) 47–64

Contents lists available at ScienceDirect

International Journal of Coal Geology

journal homepage: www.elsevier.com/locate/ijcoalgeo

Reservoir rock properties of coal measure strata of the Lower Monongahela Group, Greene County (Southwestern Pennsylvania), from methane control and production perspectives

C.Özgen Karacan *

CDC/NIOSH Pittsburgh Research Laboratory, Disaster Prevention and Response Branch, 626 Cochrans Mill Road, PO Box 18070, Pittsburgh PA, 15236, United States

ARTICLE INFO

Article history:
Received 4 September 2008
Received in revised form 16 October 2008
Accepted 20 October 2008
Available online 29 October 2008

Keywords:
Reservoir characterization
Monongahela Group
Greene County
Appalachian basin
Wellbore logs
Geomechanical properties
Permeability

ABSTRACT

The methane emission rate into an underground mine environment from overburden strata during longwall mining is impacted by reservoir and geomechanical characteristics of the coal measure rocks in the overlying strata, as well as the presence of any coal seam. The reservoir characteristics and how they change during mining potentially affect the performance of gob gas ventholes, which consequently impacts the efficiency of methane control in the mining environment.

This study presents reservoir and elastic properties of coal measure rocks in the Lower Monongahela Group in Greene County, southwestern Pennsylvania, of the Northern Appalachian Basin. Since the source of methane in this region from underground mining is located between the Sewickley coal and the Pittsburgh coal, a specific emphasis was given to this interval. Core analyses were performed in the laboratory to determine rock porosity and permeability. Geophysical logging data (gamma, density, sonic) obtained from two exploration boreholes were used for evaluating formation boundaries, shale contents, log porosities, and geomechanical properties of formations. Permeability was also calculated using density-log data and empirical equations and compared with laboratory measurements and slug tests performed in isolated intervals of boreholes. The results presented in this study can be used as data sources for reservoir studies related to the production and control of methane.

Published by Elsevier B.V.

1. Introduction

Methane inflow into mines from overburden strata during longwall mining and the production potentials of the surface methane degasification systems, mainly gob gas ventholes (GGV), are impacted by reservoir and geomechanical characteristics of the overlying strata. Core analyses and geophysical logging techniques are two of the important data sources for characterizing the geological formations. Determinations of reservoir and strength properties of the formations are important since they affect fluid flow and storage in the overburden before and after coal extraction as the stress and strain states change as a result of longwall operations.

Available coalbed methane (CBM) production literature often provides more detail on the reservoir and mechanical properties of the coal bed than on the properties of the adjacent coal measure rocks. For instance, Vaziri et al. (1997) discuss a back analysis method for strength properties of the coal seam from field measurements of wellbore cavitations and methane production. Deisman et al. (2008) give results of some unconventional geomechanical testing for coal bed reservoir well design for the Alberta foothills and plains. Beamish and Crosdale (1998) describe the relationship between coal strength and coal composition and their effects on outburst potential. Simulation studies for CBM production and coal seam degasification also are concerned mainly with the properties of the coal bed (King et al., 1986; Remner et al., 1986; Diamond et al., 1989; King and Ertekin, 1994).

Despite their lack of attention in the literature, the reservoir and strength properties of coal measure rocks are as important as the mined coal seam itself, since their properties determine gas flow paths. Lunarzewski (1998) and Noack (1998) emphasized that the influence of the deformation processes on the mechanical properties of the rock mass occurs in a micro to macro scale. During mining-induced deformations, existing and mining-induced fractures may open further. The generation and propagation of the fractures depend on the type and composition of the rocks overlying the seam. Mining processes can thus create sudden and unstable gas releases leading to potentially dangerous underground conditions which must be prevented by using a properly designed ventilation system or by employing gob gas ventholes effectively. For instance, Whittles et al. (2006) reported the results of a simulation study to predict the source and flow path of methane emissions in a UK longwall. They concluded that the geology of coal measure strata is important to determine the caving and control of methane. Palchik (2003) conducted a series of field measurements in gob gas ventholes in Torezko-Snezhnyanskaya (Ukraine) longwall mines to determine the formation of fractured zones during mining. His study showed that the location of

* Tel.: +1 412 386 4008; fax: +1 412 386 6595.
E-mail address: cok6@cdc.gov.

0166-5162/$ – see front matter. Published by Elsevier B.V.
doi:10.1016/j.coal.2008.10.005

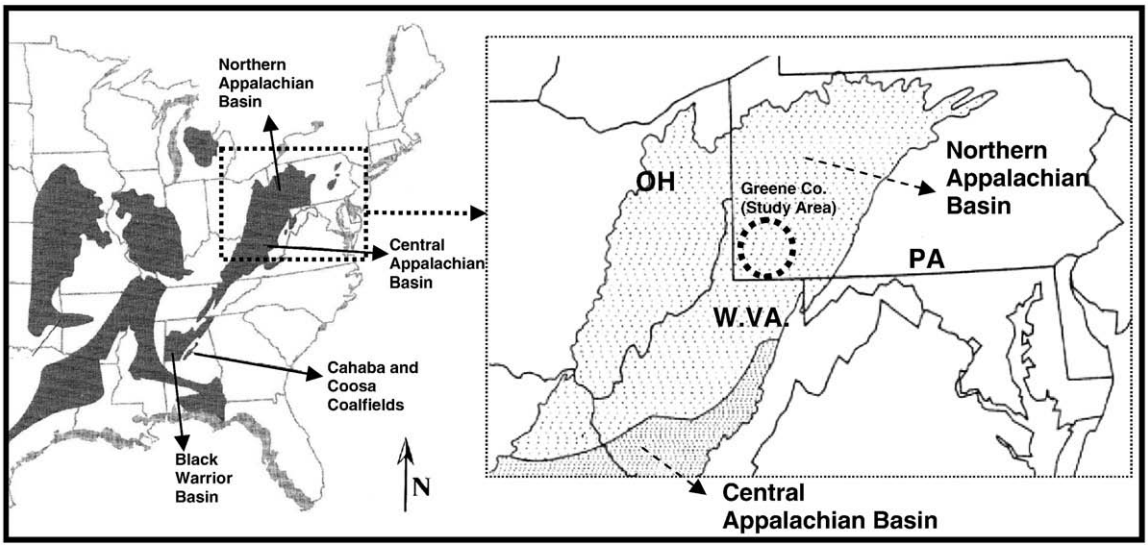

Fig. 1. Appalachian Basin and location of study area in Greene County.

fractures and gas emissions are closely related to the geology of coal measure rocks and their distances from mining activity.

In addition to the overall reservoir and strength properties, the types and thicknesses of coal measure rocks at the roof of a mined coal seam cause borehole stability problems during mining. Whittles et al. (2007) described the application of a computational model (FLAC2D) to simulate the geomechanical disturbances created due to the mining of a longwall panel at the Thoresby mine, Nottinghamshire, UK. The roof geology was considered a significant feature because it was known from previous experience that the amount of roof movement within the roadway in the region behind the coal face greatly influenced the stability and hence the gas drainage efficiency of the boreholes. An analysis of the simulation results provided a method of quantifying the effects of the geological conditions on determination of the optimum borehole spacing for the different regions of the panel.

Gas emissions and the design and stability of gob gas ventholes depend on the reservoir rock properties, the types and thickness of different layers, and the degree of their deformation dictated by their rock-strength properties. The knowledge of these rock properties is important for predicting gas emissions, sudden gas releases and changes in emission rates, as well as designing surface methane control systems. Thus, laboratory analyses of available core materials from boreholes and accurate borehole logs of coal measure rocks are important for any emission prediction and gob gas venthole design method.

This paper presents analyses on coal measure rocks recovered from the Lower Monongahela Group from exploration boreholes drilled in Greene County, Southwestern Pennsylvania (Fig. 1). Gamma ray, density, and sonic log analyses are presented to determine formation boundaries, in-situ porosities, existing fractures, and geomechanical properties (shear, Young's, and bulk moduli, and Poisson's ratio). Permeabilities calculated using log data and empirical relationships are also presented and compared with laboratory measurements and slug test permeabilities. The results of this paper are intended to serve as basic properties of coal measure rocks for site evaluations, gob gas venthole designs, and for development of numerical models for reservoir or geomechanical simulations.

2. Southwestern Pennsylvania section of the Northern Appalachian Basin

2.1. Methane sources and production potentials

The Appalachian Basin is one of the most important coal basins in the U.S. and the world's second largest coal bed methane (CBM) producing basin (Lyons, 1998). The northern part of this basin, trending in the northeast–southwest direction and occupying portions of five states (Pennsylvania, West Virginia, Ohio, Kentucky, and Maryland), is called the Northern Appalachian Basin (Fig. 1). The basin is bounded by a graben structure at the southern margins.

The Northern Appalachian Basin in southwestern Pennsylvania is a very important area for coal mining, for CBM production from coal bed degasification boreholes, and for mining-related methane (from gob and from ventilation system) emission and capture. Markowski (1998) reported that there are 24 coalbed methane pools in Pennsylvania and 11 of these 24 are located in Greene County, Pennsylvania. The main coal beds in this area are the Pittsburgh, Sewickley, and Waynesburg. Pre-mining degasification wells in this area have penetrated the Washington, Waynesburg, Uniontown, and Pittsburgh coal beds, as well as others in the Conemaugh Group (Markowski, 1998). Flows from these wells vary up to 2.8 Mm^3/day, mainly after hydraulic fracture treatment of the Pittsburgh coal seam interval. Coal mining companies are also becoming interested in converting GGVs into methane production boreholes, a practice not previously economical due to air contamination of the gob gas by the mine's ventilation system. However, with optimum drilling designed for the overlying strata and using pressure swing adsorption or a molecular gate system, gob gas can be converted economically to pipeline quality gas.

For a detailed analysis and discussion on coalbed and coal mine methane resource and production potential of the Northern Appalachian Basin, please refer to Kelafant et al. (1988), Lyons (1998), and Markowski (1998).

2.2. Coal measures of the Monongahela Group in Greene County

Greene County, located at the southwest corner of Pennsylvania (Fig. 2), is remarkable for having many productive underground coal mines. A great flat-to-dome shape of this county between two major rivers (Monongahela and Ohio) is underlain by almost perfectly flat coal seams and coal measure rocks, most of which are located in the Monongahela Group.

The Monongahela Group is located within the Pennsylvanian age sediments and includes the interval from the base of the Pittsburgh coal to the top of the Waynesburg coal. Deposition of the Monongahela Group was primarily in lacustrine and swamp environments. The Monongahela Group has a maximum thickness of about 122 m and a minimum thickness of about 76 m along the Ohio River at the southwestern edge of the basin.

Fig. 3 shows lithological logs obtained from a series of boreholes (I–VII) located along the *X*–*Y* section shown in Fig. 2. This figure also

shows the lithological logs of the two boreholes (EB-1 and 2) studied in this paper in appropriate places in relation to the *X*–*Y* section. The general coal measures in the Monongahela Group in Greene County shown in Fig. 3, and their thicknesses from top to bottom of the group, can be listed as: shale (0 to 3.6 m), Waynesburg main coal bed (1.8 m), clay (0.9 m), sandstone (6 m), limestone (1.5 m), sandstone and shale (18.3 m), Uniontown coal bed (0.3 to 0.9 m), Upper Great limestone (5.4 m), sandstone and shale (18.3 m), Lower Great limestone (16.8 m), sandy shale (12.2 m), Sewickley coal bed (0.3 to 18.3 m), sandstone (3 m), the Fishpot limestone (5.4 m), sandstone and shale (7.62 m), Redstone coal bed (0.3 to 1.2 m), limestone (3 m), Pittsburgh upper sandstone (12 m), shale (0 to 3 m), and Pittsburgh coal bed (1.5 to 3.7 m) (Penn State University Libraries, 2000).

Fig. 3 also shows that there are three main coal groups in the Monongahela Group of coal measures: Pittsburgh group of coals, Sewickley group of coals, and Waynesburg group of coals. The Pittsburgh group coals consists of the Pittsburgh coal, the Pittsburgh Rider, which is usually located 0.3–0.9 m above the Pittsburgh main coal, and the Redstone coal. The Pittsburgh coals are deepest in the center of the basin, occurring at 366 m. The group is generally persistent and consistently thick, averaging 1.8–2.4 m thick (Ruppert et al., 1999). Overlying the Pittsburgh coal by 6.1–15.2 m is the Redstone coal, which is not as extensive as the Pittsburgh. In general, the Redstone coal is 0.3–0.9 m thick when present.

The Sewickley group coals include the Sewickley coal itself and any riders and splits of the main bench when it occurs. The group underlies 20,700 km^2. Sewickley coals, which are deeper than 122 m, occupy an area of approximately 10,100 km^2. The deepest Sewickley coals are found in SW Pennsylvania at a depth of nearly 366 m. The Sewickley coal is laterally persistent and generally 0.3–0.9 m thick, although thicknesses of nearly 1.83 m were measured. Overall thicknesses for the coals show that the depositional center was located in SW Pennsylvania.

The Waynesburg Group coals are made up of the Waynesburg coal, the Waynesburg A coal, and the Waynesburg B coal. The Waynesburg is laterally persistent and is usually multiple bedded. The Waynesburg has the most limited area with about 18,100 km^2. They reach a maximum depth of approximately 244 m in the deepest portion of the basin.

3. Borehole locations, data sources, and evaluation methodology

For a preliminary characterization of reservoir properties of coal measure rocks, multiple data sources from two exploration boreholes (EB-1 and EB-2) were used. These two boreholes were drilled in two different mining areas in Greene County and were approximately 8 km from each other. EB-1 was northwest of Waynesburg and borehole EB-2 was southeast of the town (Fig. 2).

The boreholes were drilled to characterize the mine roof strata and the mining coal thickness at these locations. They were drilled from surface until the bottom of the Pittsburgh coalbed was reached and exceeded by about 9.1 m. Recovered cores were marked for depths and lithology identification. The total depths of EB-2 and EB-1 were 245 m (at the location, the top of the Pittsburgh seam was 252 m from the surface) and 263 m feet, respectively. After completion of drilling, both boreholes were logged with gamma and density tools for the entire length of the borehole, and EB-2 was logged with a full-wave sonic tool in addition to gamma and density. Table 1 shows the type of data sources and the samples obtained from each borehole.

4. Evaluation methodology for coal measure strata

4.1. Handling drill cores and laboratory core analysis

Cores from an entire interval within the Sewickley limestone and Pittsburgh sandstone (204–247 m at EB-1 location) that corresponds to the Lower Monongahela Group of coal measures were obtained during exploration borehole drilling. This interval is important for mining and methane control because it remains in the "fractured zone" during mining of the longwall panels in the area. This interval is

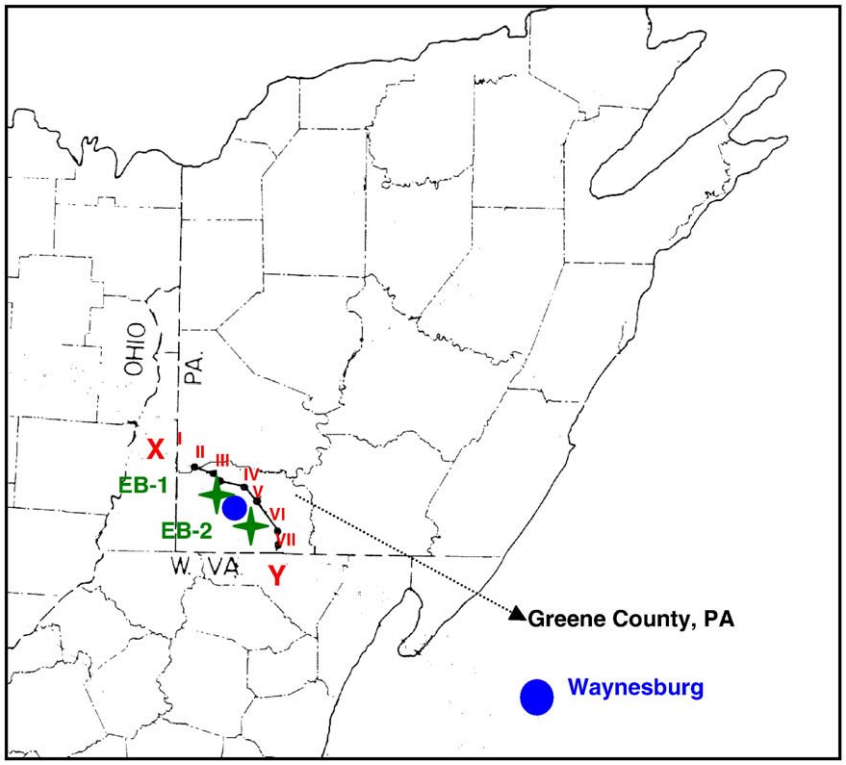

Fig. 2. Locations of Greene County and Waynesburg. Map also shows the section and locations of lithological logs shown in Fig. 3. EB-1 and EB-2 are approximate locations of the studied boreholes in this paper.

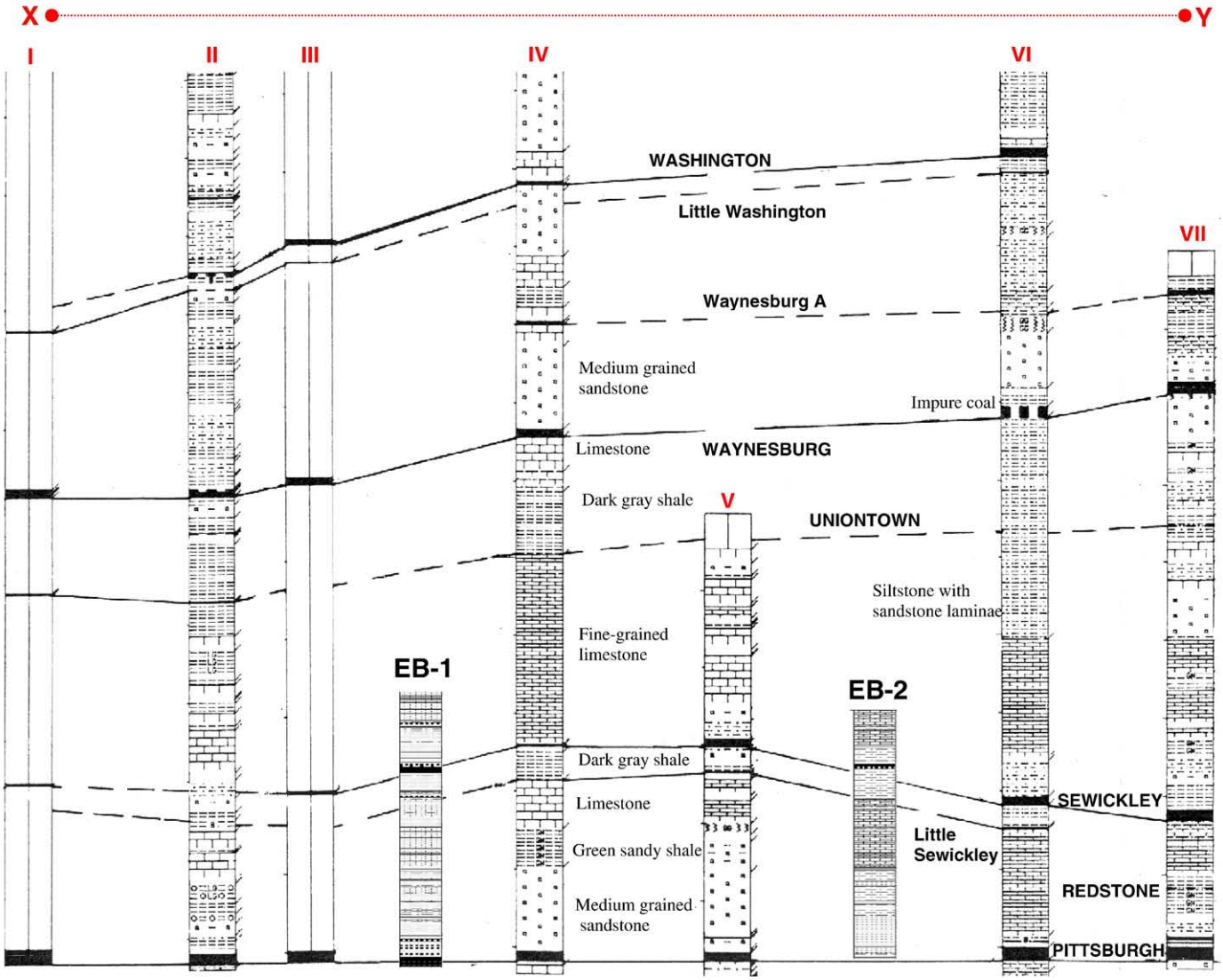

Fig. 3. Lithological logs (modified from Kelafant et al. (1988)) of the boreholes drilled in Greene County along *X*–*Y* section shown in Fig. 2. Major layers are indicated on the figure. Lithologic sections of EB-1 and 2 are also shown in appropriate places according to Fig. 2.

considered to be the source of strata gas and the location of the high-permeability fracture network for migrating methane (Karacan et al., 2007). GGVs are drilled and completed with slotted sections in this interval for capturing methane before it enters the mine environment.

Recovered cores were preserved in 7.6-cm diameter plastic sleeves after photographing and documenting the intervals to prevent dehydration and fragmentation. Preserved cores from EB-1 were later cored as plugs in the laboratory and analyzed for primary porosity and permeability. Core plug locations for sample preparation and for measurements were selected based on the integrity of the samples and on the presence of any fracturing that could create paths for methane flow into the mine environment and to the operating gob gas ventholes. A total of 23 core plugs (2.54 cm in diameter) were prepared from the drill cores. Core plugs were taken horizontal to the bedding planes, thus parallel to the natural flow direction. It was not possible to recover more plugs due to separation of rocks at fissures and formation boundaries. In fact, only 15 core plugs remained intact for further measurements of porosity and permeability.

Core plugs were dried in a low-temperature analytical oven and dimensions were measured. The grain volumes of plugs were determined using a helium porosimeter. This method yields effective matrix and micro-fracture porosity of samples.

After porosity measurements, both the core plugs and the drill cores were taken to the WV Geological and Economic Survey laboratories to measure permeabilities using a micro permeability device. Permeability readings were taken from various locations on the cores and core plugs. Micro permeability measurements were taken at eleven locations and some measurements were repeated for duplication purposes and to verify accuracy.

In order to characterize small-scale heterogeneities within the core plugs, they were scanned with a medical X-ray CT scanner modified

Table 1
Data availability from EB-1 and EB-2 boreholes

	Driller's log	Drill cores	Core plugs	Gamma ray	Density log	Full wave sonic
EB-1	☺	☺	☺	☺	☺	☻
EB-2	☺	na	na	☺	☺	☺

☺: Data measured/available; ☻- EB-1 has not been logged by sonic techniques. However a pseudo-sonic log was created using fractal statistics and radial basis functions (Karacan, 2008). Derived rock strength parameters using this approach are presented in this study. na: Cores not available.

for petrophysical studies at the DOE-NETL Morgantown facility. Core plugs were scanned with a 1-mm beam thickness along their entire lengths. Thus, each core had 30–40 images taken at 120 KeV with water-phantom calibration. These images were evaluated visually and by determining the average CT number and its statistics within a circular region of interest.

4.2. Evaluation of gamma ray (GR) logs for formation boundaries and shale volume

The GR is a record of a formation's radioactivity. The GR is usually used to identify boundaries, primarily shale units from other lower radioactivity formations (limestones, sandstones and dolomites) and to quantify shale volume. In fractured formations, an increase in the gamma ray reading without concurrently higher formation shaliness can be observed. This increase has been explained by deposition of uranium salts along the discontinuity surfaces of a fracture or within the crack itself. Also, it is not uncommon to find as much as 0.01% uranium or thorium in dark bituminous shale units, which increases the gamma ray reading (Dresser Atlas, 1974).

Fig. 4-I shows the GR log received from the EB-2 borehole, as an example, that was used to calculate shale volume.

The following equation can be used to quantify the shale volume by using GR log (Schlumberger, 1991):

$$V_{sh} = \frac{GR_I - GR_{clean\ rock}}{GR_{shale} - GR_{clean\ rock}}. \quad (1)$$

In this equation, GR_I is the gamma ray reading (cps—count per second) from the log. The other two terms are the GR readings of the clean formations (clean sandstone and limestone) and the pure shale. For calculating shale volume, the types of the formations and their thicknesses were first identified from the GR logs of boreholes EB-1

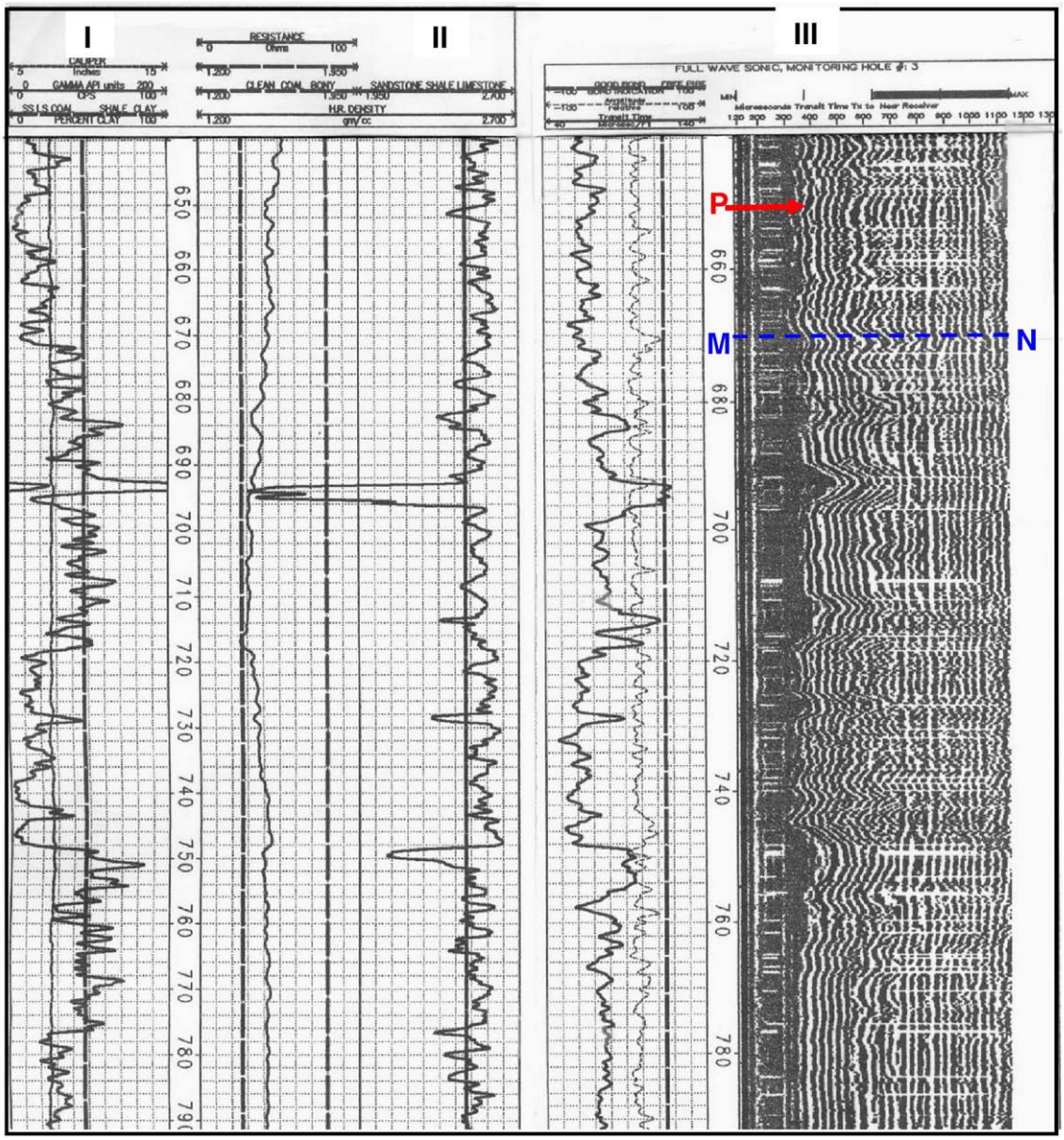

Fig. 4. Example gamma (I), density (II), and full waveform sonic (III) data obtained from EB-2 borehole. In III, "P" indicates the arrival of the compression wave to the near detector. M–N profile is the depth where the waveform shown in Fig. 5, from the near detector, was recorded.

Table 2
GR readings for isolated formations

Carb. Shale	Shale	Limestone	Sandstone	Coal
150	100	5	40	20

Units are in cps.

and EB-2. The clean-formation readings of the tool were determined by locating the clean sandstone and limestone units in the log. Pittsburgh sandstone and limestone intervals were deemed suitable for this purpose. For the shale reading, the average reading of the shale intervals was determined and used in the calculation (Table 2).

In shale volume calculations, each interval was calculated separately using the respective clean-formation reading. The aim was to minimize errors from using a single formation GR value for the entire interval.

4.3. Evaluation of density log (DL) for porosity calculation

High-energy gamma rays from a natural radioactive material are directed at the formation to interact with the rock material to measure bulk density of the formation (Schlumberger, 1991). Fig. 4-II shows the density log along with resistivity log for the EB-2 borehole that was used to calculate bulk density. Once the bulk density (ρ_b) is determined, one can calculate the porosity. However, before porosity can be determined, the lithology of the formation, the matrix density, and the fluid density filling the pore space must be known. For a clean formation of known matrix density, ρ_{ma}, with a fluid of average density, ρ_f, the linear sum of the contributions can be used to calculate porosity (ϕ):

$$\rho_b = \phi\rho_f + (1-\phi)\rho_{ma}. \quad (2)$$

There are a variety of factors affecting bulk density measurements. One of the most important ones is the shaliness of the formation. This affects the measurement by the amount of its contribution to the total signal. A correction should be made to density by the volume of shale (V_{shale}) to obtain a shale-corrected density measurement, as follows:

$$\rho_b = \rho_{b_{sh.free}}(1-V_{shale}) + \rho_{shale}V_{shale}. \quad (3)$$

In Eqs. (2) and (3), and throughout the calculation of porosity, the density values listed in Table 3 were used for individual strata intervals to minimize the errors that may arise from using a single density value for the entire interval. Shale volume is determined from the GR log.

4.4. Calculation of Young's, shear, and bulk moduli, Poisson's ratio, porosity from sonic log (SL)

Borehole EB-2 was also logged with the full wave sonic tool. The full wave sonic signature of this borehole received by the near detector within 201–241 m (660–790 ft) depth is shown in Fig. 4-III. In sonic logging, ultrasonic frequencies that create particle motions in different directions in and around the borehole are employed.

A full wave sonic tool generates three types of waves in the formation and in the borehole. In the case of a compressional wave, the acoustic wave alternately compresses the surrounding medium on a forward movement and rarifies it on a backward movement. The shear wave is a transverse wave in which the direction of propagation is perpendicular to the direction of particle displacement. Solids have a tendency to oppose shearing forces which cause particles to slide relative to each other. Shear waves cannot travel through them. On the other hand, the Stoneley wave is a type of large-amplitude surface wave generated by a sonic tool in a borehole. Stoneley waves can propagate along the walls of a fluid-filled borehole. When the borehole crosses permeable zones or fractures, some fluid movement occurs between these locations and the borehole. This results in some energy loss of the wave (Endo, 2006). Thus, analysis of Stoneley waves can define the locations of fractures and estimate the permeability of the formation.

Fig. 4-III displays the full waveform, transit time, and amplitude received at the near detector for EB-2 within 201–241 m. In the receiver, the *P* waves arrive first, the shear wave arrives next, and the tube wave traveling up the borehole water column arrives third. Shear wave and tube wave (Stoneley wave) transit times can be determined by analyzing each of the individual wave forms for second and third arrivals. Long transit times for the first break, compressional wave (*P* wave) arrivals, indicate slow formations, while small transit times indicate fast formations. Only the arrival of the compression wave shows up in the full waveform clearly (*P* in Fig. 4-III). The shear and tube wave arrivals are read from the individual wave forms, 10 of which were collected for each 30.5 cm of the borehole. Thus, for the 201–241 m interval, 1300 wave forms were analyzed. The full wave form in Fig. 4-III is a plot of the individual wave forms stacked side by side, with the peaks as white and the troughs as black. A sample individual waveform from the near (along the M–N profile in Fig. 4-III) and the far detectors is given in Fig. 5. In this figure, the intervals show where compression, shear, and tube waves arrive at a particular depth.

Acoustic travel time measurements of subsurface formations can be interpreted in terms of formation porosity. A unit volume of rock through which the acoustic wave travels is influenced by the total make-up of that rock. The measurement recorded on the log is the sum of the effects of the solid part of the rock and the fluid-filled pore space.

In this study, the following relationships were used to calculate porosity of the formations with shale correction:

$$\phi = \frac{\Delta t - \Delta t_{matrix}}{\Delta t_{fluid} - \Delta t_{matrix}} - V_{sh}\frac{\Delta t_{sh} - \Delta t_{matrix}}{\Delta t_{fluid} - \Delta t_{matrix}} \quad (4)$$

where Δt is the interval travel time of the compressional wave, which was determined from the full wave sonic record (Figs. 4-III and 5) based on the first arrival wave, and V_{sh} is the shale volume obtained from GR-log analysis (Eq. (1)). Since the compressional wave travels almost twice the velocity of other waves, its arrival is undistorted by later arriving waves.

Before using this equation for calculating porosity, it is necessary to have values for the rock matrix (Δt_{matrix}) and the formation fluid (Δt_{fluid}). In this case, the formation fluid was assumed to be water. The interval transit time in the rock matrix will vary considerably depending on the formation type. To be more specific, Δt_{matrix} changes with variations in the chemical composition of the rock and also its compaction (Castagna et al., 1985; Bemer et al., 2004). The selection of proper matrix velocity to be used in the porosity calculation requires knowledge of the lithology of the sections being investigated. This information was gathered from the driller's log and the lithological log of EB-2. In Eq. (4), the velocity values for different strata given in Table 4 were used along with the interval transit times to calculate sonic porosity.

Besides porosity, velocities obtained from full wave sonic logs (Fig. 4-III) can be used as the fundamental information for rock classification and geotechnical evaluation. Acoustic travel time of any type of ultrasonic disturbance is explicitly tied to the density and the elasticity of the medium. In this work, shear modulus and Young's modulus were calculated using the velocities of compressional and shear waves determined from the sonic log.

Table 3
Bulk density readings for individual minerals

Mixed clay	Limestone and dolomite	Sandstone	Coal	Water
2.5	2.8	2.65	1.35	1.0

Units are in g/cc.

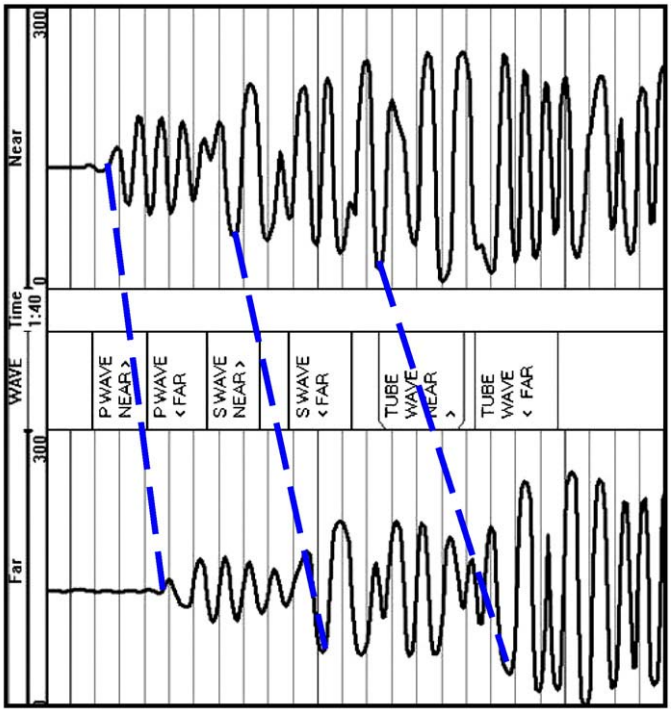

Fig. 5. Example sonic waveforms recorded at the near and far detectors during logging of EB-2 at 204 m depth (M–N profile in 4-III). Figure also marks the arrivals of three different waves to these detectors.

Compressional waves are characterized by first arrival times. Although slower than compressional waves (0.5–0.7 times), shear waves are usually stronger and can be identified in the total wave train. Both of these waves and the calculated velocities were used in the following equations for calculation of Young's and shear moduli (Takahashi et al., 2006).

$$G = \rho V_s^2 \tag{5}$$

where ρ is the density, G is shear modulus, and V_s is the shear wave velocity.

Dynamic Young's modulus was calculated using both compressional and shear waves and a determination of dynamic Poisson's ratio (σ):

$$\sigma = \left\{ \left(\frac{V_p}{V_s}\right)^2 - 2 \right\} \Big/ \left\{ 2\left(\frac{V_p}{V_s}\right)^2 - 2 \right\} \tag{6}$$

where V_p and V_s are the compressional and the shear wave velocities. Young's modulus (E) can thus be calculated using

$$E = 2G(1+\sigma). \tag{7}$$

Using Eqs. (6) and (7), the bulk modulus (K) can be calculated using Eq. (8):

$$K = \frac{E}{3(1-2\sigma)}. \tag{8}$$

5. Results and discussion

5.1. Borehole cores, porosity, and permeability from laboratory measurements

The core pictures at various depths of EB-1 show the heterogeneity of the strata in terms of layering and coal measure rock types (Fig. 6a–t). Green and gray shales are abundant in large intervals and occasionally mixed with sandstones, probably decreasing their strength and reservoir quality in these intervals. Shale layers are extensively fractured (some of them due to drilling and coring) and usually separated at the interfaces from stronger units. When present, limestone appears to be relatively free of shale and forms a consistent and strong layer. There are no apparent pores or macro-scale primary porosity systems in the interval. However, cores show frequent fractures, most of which are parallel to the bedding and occur at formation boundaries.

Table 5 shows the results of porosity measurements by helium porosimeter. The measurements show that some of the core plugs had minimal porosities between 1 and 2%. A couple of cores taken at 233.8–234.1-m drill depths in the borehole had higher porosities of ~6% and ~11%.

Permeability readings were taken from various locations on the cores and core plugs. Micro permeability measurements were taken at eleven locations and some measurements were repeated for duplication purposes and to verify accuracy. The measurements were performed by forcing the measurement probe to the rock surface under unconfined conditions. The measurements were conducted at laboratory temperature conditions (~25 °C). The results are given in Table 6 and show that for the core intervals, the measurements indicated generally low permeabilities, except at 217.3 m and 224.6 m. These comparably higher values of permeability are attributed to the hair-like fissures observed on the samples. Since the fissures and fractures were not included in the samples, it should be mentioned that the porosity and permeability measurements would represent

Table 4
Formation velocities used in Eq. (4)

Mixed clay	Limestone	Sandstone	Coal	Water
328.1	157.5	173.9	295.3	715.2

Units are in μsec/m (Dresser Atlas, 1974).

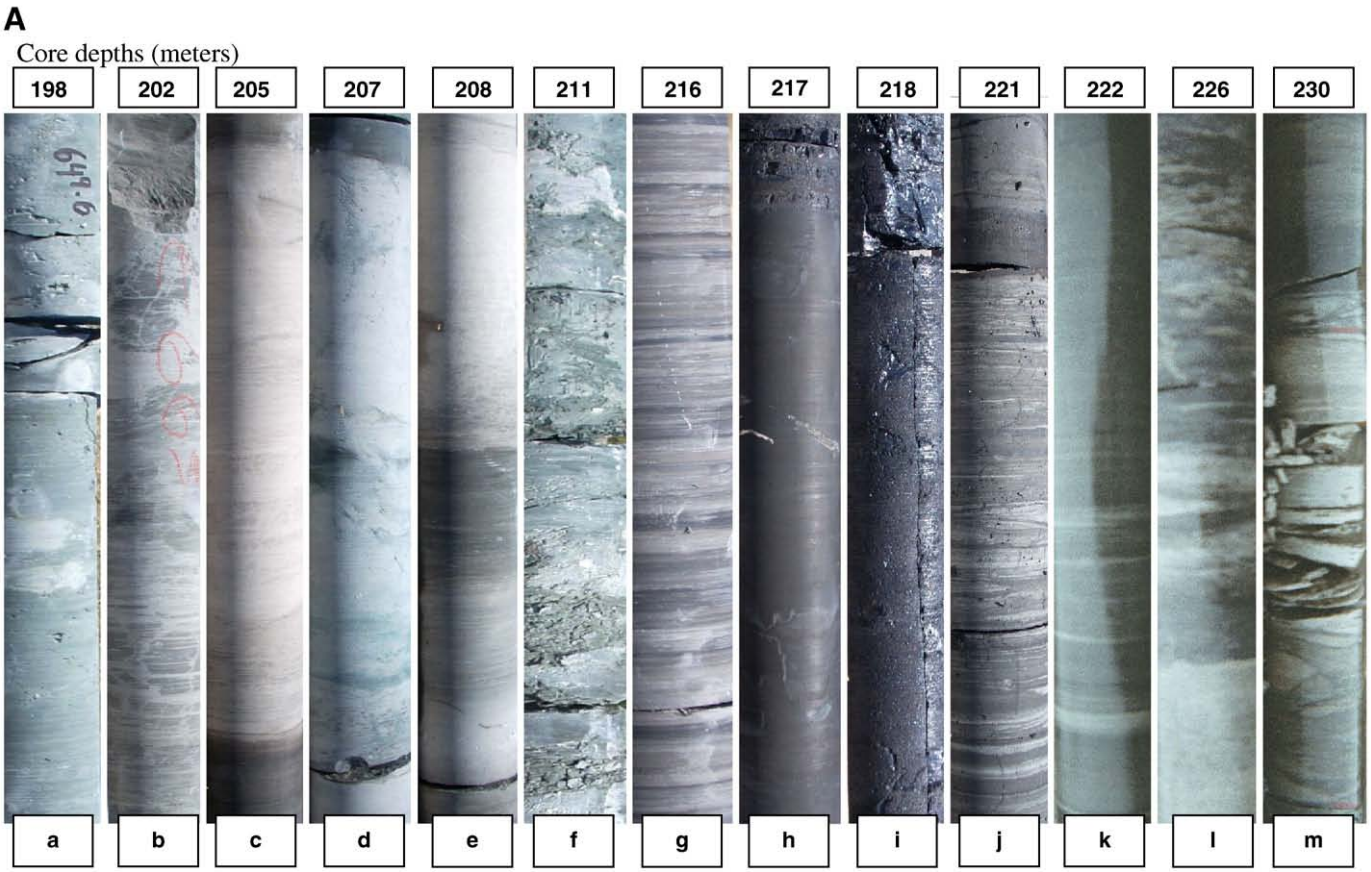

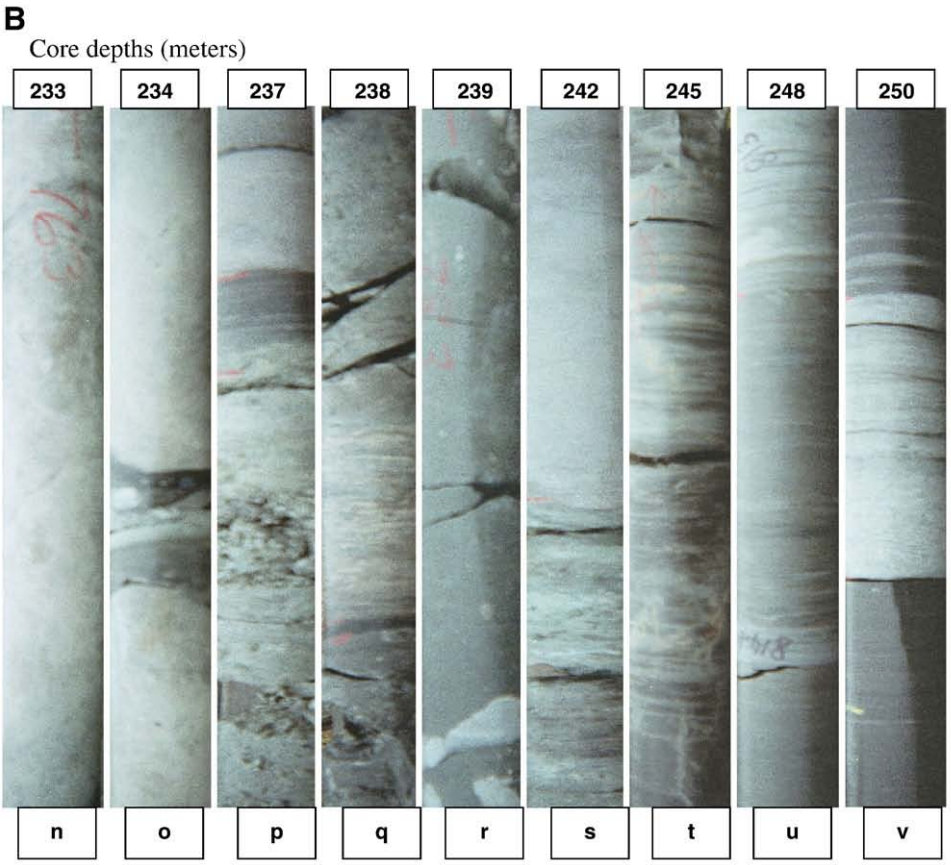

Table 5
Laboratory porosity measurements on core plugs obtained from EB-1

Number	Sample depth (m)	Length, cm.	Diameter, cm.	Bulk volume, (cm^3)	Grain volume, (cm^3)	Porosity, fraction
1	226.5	3.8	2.5	18.3	18.0	0.019
2	227.4	3.8	2.5	18.3	18.1	0.011
3	233.5	4.2	2.5	20.2	19.6	0.027
4	233.8	3.5	2.5	16.8	15.9	0.056
5	234.1	3.4	2.5	16.6	14.8	0.111
6	241.7	3.6	2.5	17.5	17.4	0.006
7	241.9	4.0	2.5	19.5	19.4	0.002
8	242.0	3.7	2.5	18.2	18.2	0.001
9	243.8	3.5	2.5	17.0	16.8	0.012
10	247.2	3.8	2.5	18.3	17.9	0.019
11	247.8	3.9	2.5	18.8	18.6	0.013
12	248.1	3.9	2.5	18.9	18.4	0.026

rock-matrix values, excluding the effects of fractures on storage and flow properties of the formations.

After laboratory testing of porosity and permeability, core plugs were scanned using an X-ray CT scanner. X-ray CT is a non-destructive technique which detects the attenuation of X-rays passing through an object, which is dependent on bulk density and effective atomic number. X-ray attenuation is mapped in Hounsfield units, or in CT numbers, in each voxel of a CT image of the object. The CT numbers can be converted to density using a calibration function. If a water phantom is used, as in this study, the CT number is 0 for water (1 gr/cc) and −1000 for air (negligible density). The principles of X-ray attenuation are given in Ketcham and Carlson (2001) and in Karacan and Mitchell (2003).

In this study, the average and the maximum CT numbers determined in a circular region of interest were plotted for all the images taken for each core (Fig. 7). Example images from four different core plugs in the borehole are also shown in this figure. The scatter plot shows the heterogeneity in the cores. If the maximum (or minimum) and the average CT numbers accumulate within a small range of values, then the rock at that scan location is homogeneous (e.g., 226.4 and 234.1 m). However, if the values are widely scattered, then it indicates the existence of heterogeneities within the cores (e.g., 243.8 m). The plot and the images show that the core plugs have small-scale heterogeneities (243.8 m, 247.2 m, 248.1 m) that may not be discernible from visual inspection of borehole cores or from the analysis of well logs. However, these heterogeneities may affect flow characteristics within the formation and flow and strength tests conducted in the laboratory.

5.2. Geophysical log evaluations

Gamma ray and density logs are two of those techniques that are most frequently used in the field for conventional and unconventional reservoir evaluation studies. Full wave sonic logs, are more expensive to run, data-intensive, and more complicated in terms of operation procedures. However, they provide more detailed information about the condition of the borehole and surrounding strata, such as geomechanical parameters and formation permeability (Qobi et al., 2001; Takahashi et al., 2006; Yan, 2002; Milkereit and Ji, 2005; Castagna et al., 1985). In this section, gamma ray (GR), density (DL), and sonic logs from EB-1 and EB-2 were evaluated to determine porosity, shale volume, and geomechanical properties of the coal measure rocks.

5.2.1. Strata thickness, lithology and GR and DL readings

DL and GR were used to identify formation boundaries, to calculate porosities, bulk densities, and shale volumes, and to create lithological logs of the formations in EB-1 and EB-2. Calculations were based on the methods described in Sections 4.2 and 4.3 using the raw data shown in Fig. 4-I and -II. In order to create lithological logs, ALT's WellCAD v4.2 (Advanced Logic Technologies, 2008, Luxemburg) was used. In addition, strata thicknesses recorded during drilling were plotted based on the recovered cores.

Fig. 8 shows the lithological log, thicknesses of major layers defined from the driller's log, and the values of gamma and density readings from EB-2. At this location, the top of Pittsburgh coal bed was at a depth of 252 m. The general sequence between 204 m and 241 m, which was to remain in the fractured zone during mining above the Pittsburgh seam layer, was divided into four horizons (dotted lines in Fig. 8). These zones are mainly alternating sequences of limestone and shale and sandstones, as concluded from GR and DL. In each of these zones, thin shale layers (A, C–F) are sandwiched between stronger limestone or sandstone formations. In this log, the Sewickley coalbed is located at “B” (low gamma ray, low density) and overlain by carbonaceous shale (A), which records a high gamma ray reading accompanied by a decreased density.

GR and DL, as well as lithological logs and strata thicknesses for EB-1, are shown in Fig. 9. At this location, the Pittsburgh coal bed is found at a depth of 254 m. A similar sequence of layers, as in EB-2, is also observed at this location. Limestone layers are separated by shale layers as annotated on gamma and density logs (A–G). Some of the low density readings (A* and B*) are associated with carbonaceous and limy shales and with highly porous shale units. At this borehole site, the Sewickley coal seam is thicker than it is at the EB-2 location. This might influence the amount of methane that will be experienced once this location is undermined. Also, this location is missing the thick Pittsburgh sandstone that overlays the Pittsburgh coal seam. The absence of this layer may affect the fracturing and the amount of methane associated with this layer.

5.2.2. Shale content and porosity of formations at EB-1 and EB-2 using GR and DL

In order to calculate shale volume and porosity using GR and DL, the types of the formations and their thicknesses were first identified (Figs. 8 and 9). The clean-formation readings for each rock type were determined by locating the clean sandstone and limestone units in the logging data. Pittsburgh sandstone and limestone intervals were suitable for this purpose, since they were mostly free from shales. The GR reading for coal was determined based on the average GR reading along the Sewickley layer. For the shale GR reading, the average reading of the shale intervals was determined and used in the calculations (Eq. (1)) given in Section 4. Porosities were calculated based on a similar procedure given for GR by using DL (bulk density) with shale corrections given by Eqs. (2) and (3).

Fig. 10 shows the shale contents and porosity values for EB-1. The calculations show that the lowest shale percentage is found in limestone-bearing units at depths of 225.5 m, and 230.1–234.7 m, with an average shale content of 5–10%. Within this interval, there are layers of weak shale formations at around 229.9 m and 233.5 m. These and similar layers are potentially weak interfaces to be affected by stresses during mining and by resulting bedding plane separations.

Fig. 6. Cores recovered from EB-1 during drilling and their recovery depths (in meters). a - limestone with shale, b - green shale, c - limestone with dark shale, d - limestone with green shale, e - limestone with dark shale, f - limy shale, g - sandstone with gray shale, h - black carbonaceous shale, i - Sewickley coal, j - gray shale with sandstone streaks, k - shale with sandstone, l - limestone with shale, m - limestone with gray-black shale, n - limestone, o - limestone with shale layer, p - limestone with limy shale, q - sandstone with gray shale, r-green limy shale, s - limestone, green limy shale, t - green sandy shale, u - sandy shale, v - black shale and sandstone.

Table 6
Laboratory permeability measurements on core plugs obtained from EB-1

Number	Sample Depth m.	Measurement No.	Permeability md.
1	212.1	1	0.499
1	212.1	2	0.503
2	217.3	1	2.484
2	217.3	2	2.463
3	220.4	1	0.207
3	220.4	2	0.204
4	224.6	1	6.616
4	224.6	2	6.557
4	224.6	3	6.210
4	224.6	4	6.171
5	226.5	1	0.093
6	227.7	1	0.153
7	233.8	1	0.122
8	234.1	1	0.153
9	234.5	1	0.132
10	247.8	1	0.380
10	247.8	2	0.333
11	248.1	1	0.606
11	248.1	2	0.530
11	248.1	3	0.291

Outside of limestone intervals, the average shale content in the strata varies from 40 to 50%.

Fig. 10 also shows the porosity values calculated in the EB-1 borehole using the density log. This plot shows that porosity values are generally low (0–0.1), except for some intervals where values exceeding 0.5 are observed. These locations are at 210.3 m (A), 217.9 m (B), 224.0–225.5 m (C–D), 233.1 m (E), 237.8 m (F) and 243.8 m (G), of which 224 m corresponds to the Sewickley coal bed. These intervals are generally associated with fractures, laminated layers, and shales interlayered between limestone units. These high porosities can result in weak spots in the strata that may fracture and separate, as well as promote methane flow towards any borehole or the mine environment. These areas may potentially be the reservoirs of free methane that will flow into a pressure sink once the fracture connection is established during mining.

Similar observations can be made for EB-2 based on clay content and density porosity (Fig. 11). In this borehole, average shale content in sandy-shale layers is around 40%. Higher shale-content areas are interbedded with a more competent limestone sequence and Pittsburgh sandstone between 217.9 and 228.6 m and below 236.2 m, respectively. The layer that is almost exclusively shale at 211.8 m is closely associated with thin carbonaceous shale and is either a clay-filled fracture or a fracture surface that is carrying a high amount of radioactive ions.

The calculated porosities for EB-2, based on the density log (DL), indicate that most porosity values are 0.1 or less (Fig. 11). However, there are higher porosity sections based on the strata. The highest values are marked from A to H on the figure. They are generally associated with shale layers, especially where the clay content is high and possibly where some natural fractures within the strata or along the bedding interfaces are present. In these sections, porosities were as high as 0.4–0.5 and, in some instances, even more. These high-porosity areas constitute weak spots for strata fracturing that create high permeability pathways and pockets for free methane.

5.2.3. Porosity evaluation using sonic log (SL)

In order to separate possible natural fractures in the interval of interest from its primary porosity, the sonic log (SL) of EB-2 was used. Porosity calculations using sonic log data are discussed in Section 4 and given as Eq. (4). The difference between these two methods for calculating porosity is due to the nature of the response measured in the formations: the DL is responsive to all pores of all sizes, including

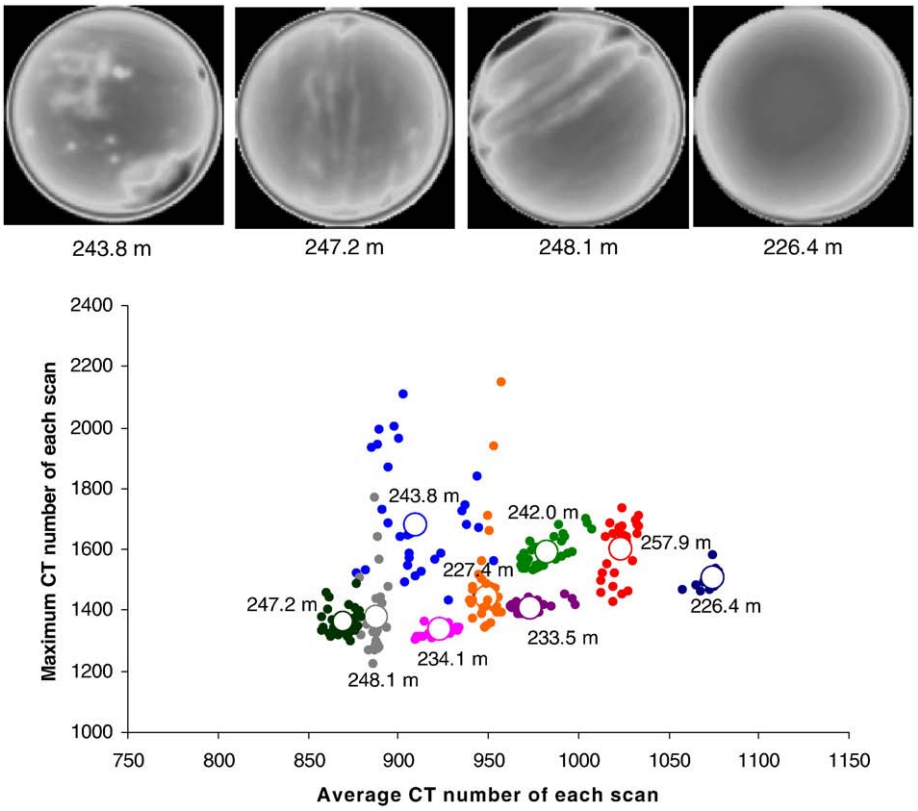

Fig. 7. Sample CT images from core plugs and a plot of average versus maximum CT number determined from the core images. Large symbols are the averages of "average CT numbers" and "maximum CT number" for each core.

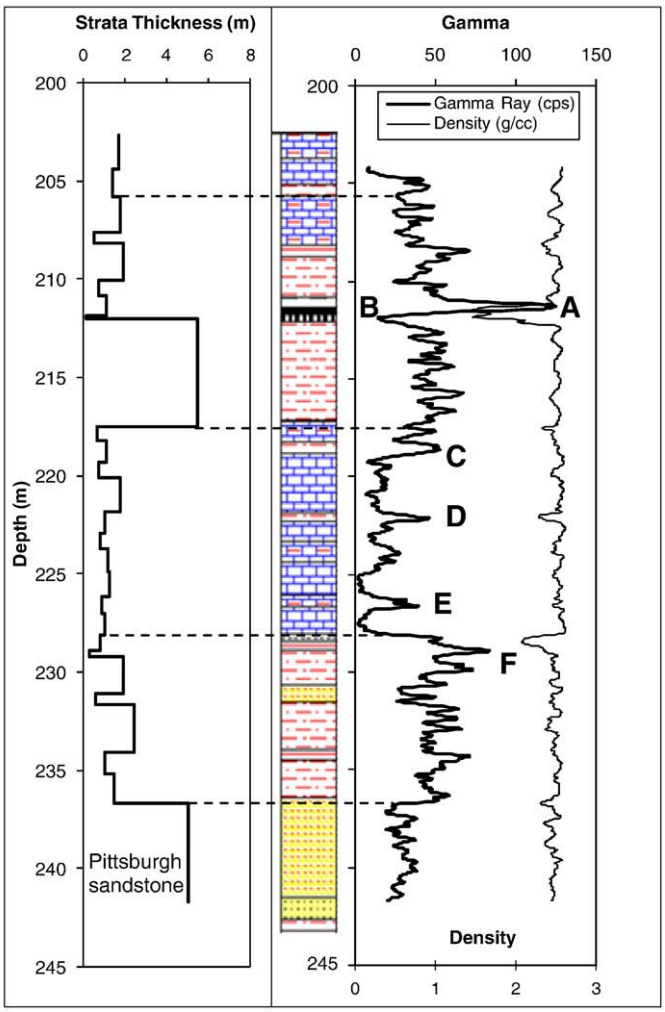

Fig. 8. Lithological log, thicknesses of major layers defined from driller's log, and GR and DL readings from EB-2.

fractures. However, field observations over many years have shown that the SL is a measure of primary porosity but largely insensitive to secondary porosity as fractures or vugs. This discrepancy arises from the sonic tool measuring the transit time by recording the first arrival waveform which often corresponds to a route in the borehole wall free of fractures and vugs. Thus, comparing SL porosity to DL porosity or calculating secondary porosity index ($SPI = (\phi)_{DL} - (\phi)_{SL}$) may differentiate primary and secondary porosity (Schlumberger, 1991). In the SPI equation, $(\phi)_{DL}$ and $(\phi)_{SL}$ are density log and sonic log porosities, respectively.

Fig. 12 shows SL porosity and SPI calculated for EB-2. As can be seen from the SL porosity plot, there is a clear decrease in porosity compared to DL porosity shown in Fig. 11. The average value of SL porosity along the entire logged interval is 5.5%, with some lower and higher local deviations from this average. Particularly, points A–D are of interest due to higher primary porosities. These points correspond mainly to strata interfaces and may result from rock gouges in the fractures since they are picked up by sonic log. On the other hand, the average of DL porosity (Fig. 11) for the same interval is 0.152. The difference in average DL and SL porosity is the average of SPI, which indicates that the interval had approximately 0.1 average secondary porosity due to major fractures and vugs that the sonic log ignored. The large deviations from this average (E–J) correspond to limestone-shale and sandstone-shale or -shaly sand interfaces and are most likely due to open fractures at the interfaces. There are also some peaks above the average values within layers, which may be due to fracture networks in those layers.

The existence of these fracture signatures is important due to their potential role as a source of free methane under reservoir pressure and also as potential pathways for methane flow within the formation as the longwall face approaches. They are also important for drilling and cementing of gob gas ventholes in the area due to their potential for creating drilling fluid or cement mixture losses into the formation.

5.2.4. Evaluation of sonic logs for geomechanical properties of rock formations

Young's, shear, and bulk moduli, and Poisson's ratio for EB-2 were calculated based on the method detailed in Section 4.3. Moduli and Poisson's ratio properties of borehole strata are shown in Fig. 13. In order to make geomechanical properties of different strata intervals more distinctive from each other, the arithmetic averages of the values within different lithology intervals shown in Fig. 8 were calculated.

Young's modulus is a measure of the stiffness of a material for deformation. It describes the rock's response to linear strain. Shear

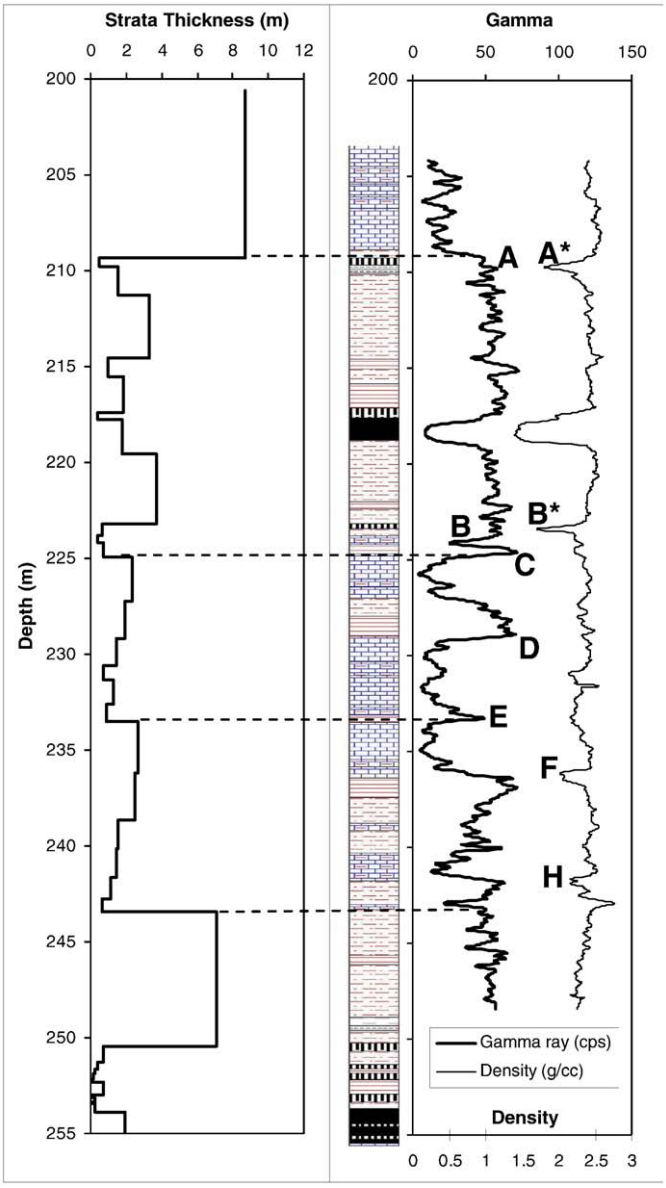

Fig. 9. GR and DL, as well as lithological log and strata thicknesses for EB-1.

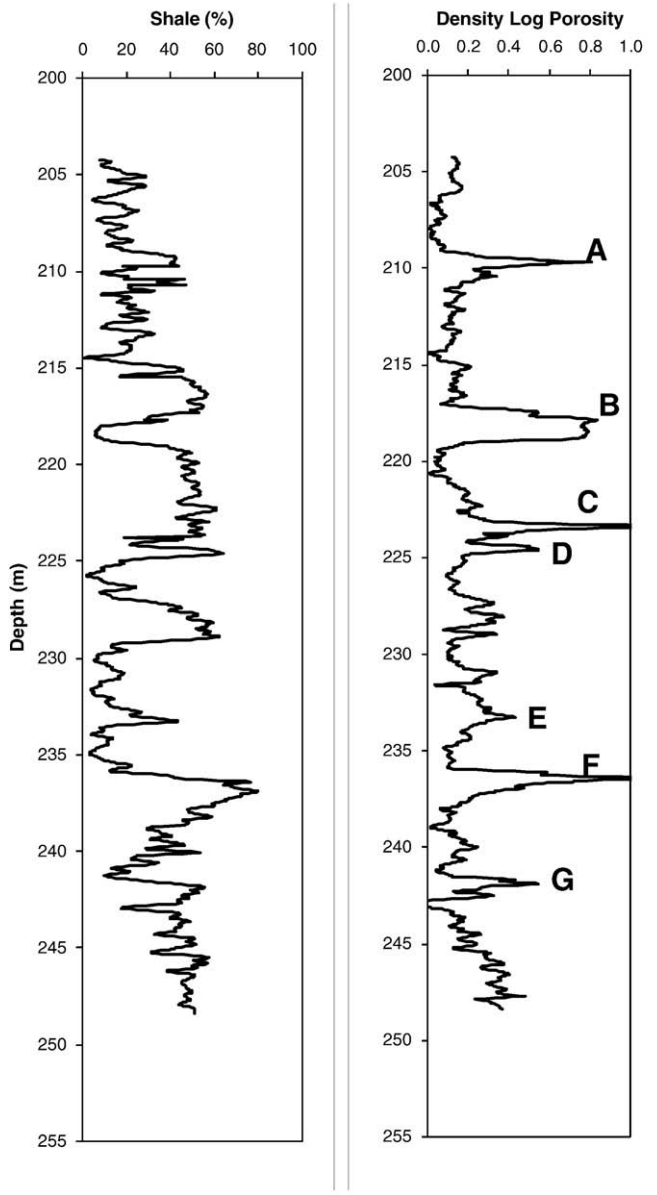

Fig. 10. Shale content and density porosity log calculated from GR and DL of EB-1.

modulus, or modulus of rigidity, describes the deformation of a rock when it experiences a force parallel to one of its surfaces while its opposite face experiences an opposing force, i.e. rock's response to shearing strains.

Fig. 13 shows that the highest Young's and shear moduli are associated with limestone and competent sandstone layers. The values in these layers are as high as 4 and 9 GPa for shear and Young's moduli, respectively. When there is a shale layer, sandy or limy shale, or coal, values decrease abruptly to values as low as 1–2 GPa, indicating weaker rock units that will be deformed easily when subjected to high stress and strain conditions that can prevail during mining. These weak layers and their interfaces with stronger rocks are candidates for easy fracturing and bedding plane separations that form increased permeability pathways for methane migration, as discussed by Palchik (2005). It should also be noticed that shear and Young's moduli are also related to density and gamma ray readings shown in Fig. 8.

The bulk modulus of a substance measures the resistance to uniform compression under hydrostatic pressure. The reciprocal of the bulk modulus is the compressibility of the substance. If a rock material is incompressible or has very little compressibility under hydrostatic pressure, its bulk modulus will be large and thus compressibility will be small. Fig. 13 shows that the bulk moduli of limestone intervals in Fig. 8 have the highest values, indicating their low compressibility compared to shale and sandy shale layers which appear to be more compressible under uniform pressure.

Poisson's ratio is the ratio of expansion in one direction of a rock caused by a contraction at right angles. The Poisson's ratio of most materials is between 0.0 and 0.5. If the material is showing almost no Poisson contraction as a response to extension, then the Poisson's ratio is 0. On the other hand, a perfectly incompressible material deformed elastically at small strains would have a Poisson's ratio of 0.5. Rocks are subject to Poisson's effect under stress and strain. For instance, excessive erosion or sedimentation in the overburden can either create or remove large vertical stresses on a particular rock layer, under which it will deform in the horizontal direction as a result of Poisson's effect. This change in strain in the horizontal direction can affect formation of joints or local stresses in the rock. Fig. 13 shows that the Poisson's ratio is between 0.1 and 0.3 for the rock layers of interest. Limestone layers are close to a value of 0.3, whereas sandstone is 0.25, and sandy shale and shale layers are between 0.15 and 0.2. These data indicate that none of the layers are perfectly incompressible and will tend to show Poisson effects as a result of changes in stress in one direction. However, this change will tend to occur more in shale and sandy shale layers. Since there will be a discontinuity in this effect in the rock layer interfaces, the likelihood of developing bedding plane separations and fractures will be higher in those regions.

A similar analysis was performed for EB-1. However, a sonic log was not run in this borehole. In order to provide operators, who do not

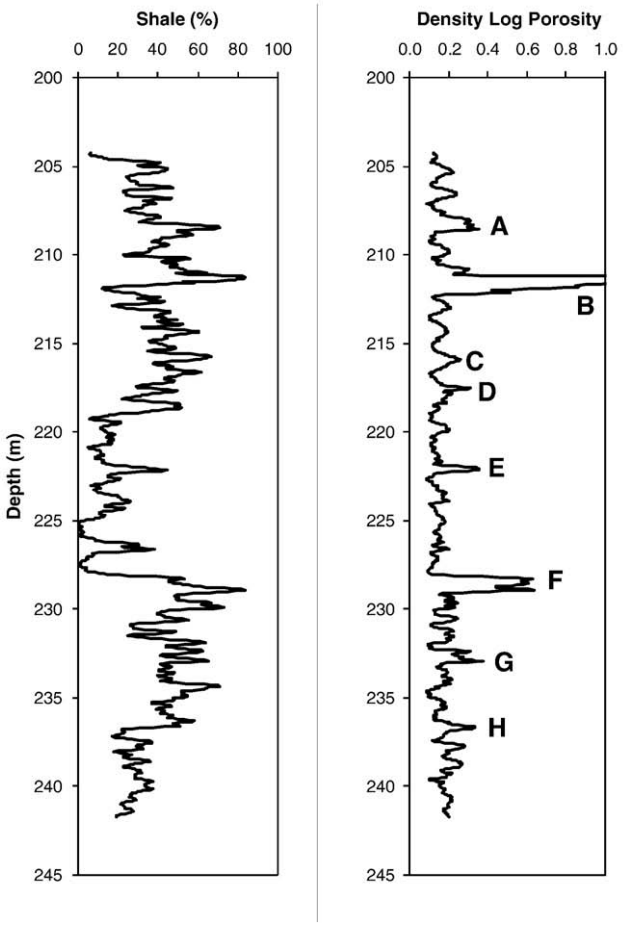

Fig. 11. Shale content and density porosity calculated from GR and DL of EB-2.

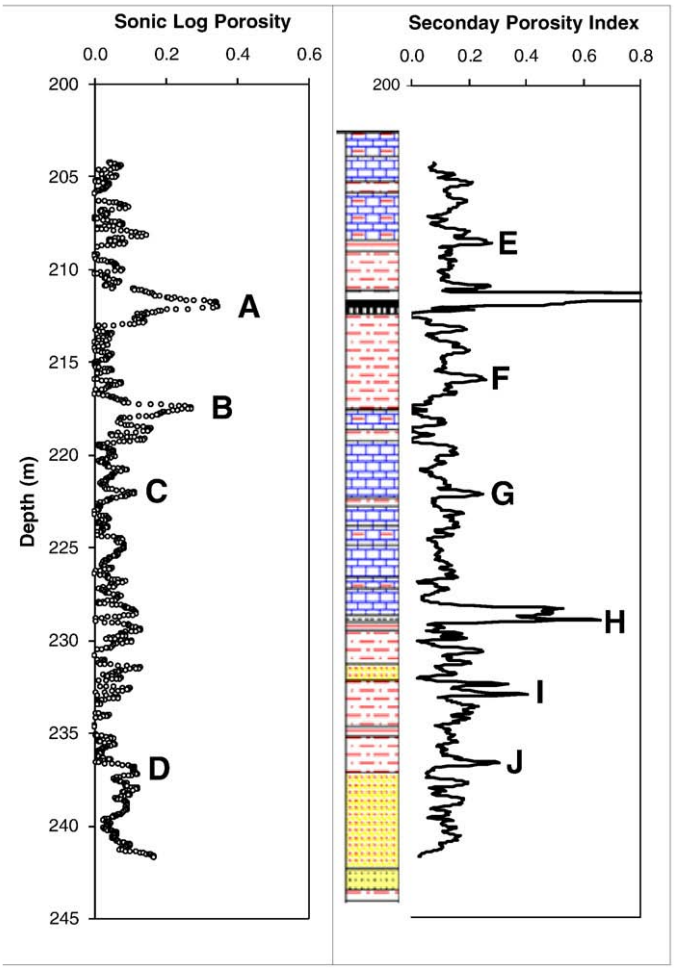

Fig. 12. Comparison of SL porosity and SPI, and with the lithologic log for the EB-2 site.

run sonic log on a regular basis (at least for coal mining purposes) due to its cost and data-intensive nature, with a simpler way of generating geomechanical properties, a new methodology was developed using gamma and density logs (Karacan, 2008). This methodology relied on the indirect effects of density and shale content of rocks on their geomechanical properties. The methodology processed gamma and density logs using Fourier transforms and fractal techniques such as fractional Gaussian noise (fGn) and fractional Brownian motion (fBm). These methods determined the similarities in data ordering while eliminating noise and then used radial basis function (RBF) networks to calculate the Young's and shear moduli of the formations. Details of this technique are given in Karacan (2008). The data presented in Fig. 14 were generated using this technique on the EB-1 borehole's gamma and density logs and its lithology log shown in Fig. 9.

Fig. 14 shows that the highest Young's and shear moduli are associated with limestone layers, as in EB-2. The values in these layers are as high as 2.5 and 6 GPa for shear and Young's moduli, respectively. The difference in these values compared to those of EB-2 may be due to the generally higher shale content and DL porosity observed in this borehole (Fig. 10) compared to EB-2 (Fig. 11). Shale, sandy shale, limy shale, carbonaceous shale, or coal have lower Young's and shear moduli as observed in EB-2, indicating weaker rock units compared to the intervals abundant in limestones. These weak layers and their interfaces with hard rocks will be deformed and separated easily at this location during longwall mining.

Fig. 14 also shows that the bulk moduli have the highest values of 4 GPa in limestone intervals and the lowest values in carbonaceous shale and coal intervals. Also, these layers, except the Sewickley coal layer, have a lower Poisson's ratio (0.1–0.15) compared to limestone layers (0.25). The higher Poisson's ratio calculated for the coal at this location may be due to lower amounts of shale calculated for this interval and possibly drilling-induced fractures observed in the coal layer (Fig. 6-i). Silitonga and Siahaan (2005) reported, based on experimental and theoretical results, that additional fracturing of a fluid-filled formation will increase the Poisson's ratio deduced using the sonic log. This is due to a slight decrease in compressional wave velocities in additional fractures compared to a significant reduction in shear wave velocities (Schlumberger, 1991).

5.3. Permeability of coal measure formations

Permeability is a critical parameter for any formation, both for economically and effectively producing fluids (production of gas, oil, or water) and for controlling the flow of those fluids to any restricted environments, such as the underground mining environment. There are various permeability models in the literature relating log or core porosity, water saturation, particle size, and log resistivity to permeability. Some of these models are reviewed in Balan et al. (1995). Sonic velocities, particularly the dispersion and attenuation of Stoneley waves, are also used to calculate the permeability of formations, especially in fractured zones (Qobi et al., 2001; Endo, 2006). This method requires obtaining high-fidelity monopole waveforms at low frequency over a sufficiently wide frequency range (Norris, 1989; Endo, 2006), necessitating a detailed procedure.

In coal measure formations that may also contain strata methane, the abundance of shales, clays, and their mixtures with sandstones and limestones make them different from formations in oil and gas reservoirs, which contain clean sandstones or fractured limestones. In coal measure rocks, the lack of primary porosity and abundance of shales/clays affect both the permeability in these formations and the sealing of thin fractures upon swelling after hydration (Hatherly et al., 2005). Each of these is important for methane control during mining.

Core pictures shown in Fig. 6 and laboratory measurements of porosity and permeability on these cores (Tables 5 and 6) prove that this is not the case in almost all layers examined within the entire coal measure interval at the EB-2 location. These pictures and tests show that the matrix is fine-grained, with very low porosity and permeability values. Thus, possible flow paths can be the existing fractures in the formation that are observable from the pictures (some of which may be related to drilling). The possible fractures and intervals that are amenable for bedding separation and fracturing were evaluated using log data in the previous sections.

In this study, permeability of the coal measure interval between the Sewickley and Pittsburgh coal seams was evaluated by two approaches. The first approach performed slug tests in isolated intervals in three underground monitoring boreholes drilled at different depths. These boreholes were 15.2 from each other and thus virtually drilled in the same formations with similar thicknesses. The second approach used empirical relationships to determine permeability for shaly formations (Yan, 2002) and sandstones (Timur, 1968). Fig. 15 shows a picture from the monitoring site and the boreholes tested using slug-test approach.

5.3.1. Slug tests in boreholes for calculating permeability

These tests were conducted in three different boreholes drilled at the EB-2 location shown in Fig. 2. The first borehole was drilled to a depth of 220 ft and completed with a 9-m slotted casing at the bottom. The second borehole was drilled to a depth of 230 m and completed with a 6-m slotted casing. The third and the deepest borehole was the "EB-2" borehole that is reported in this study. This borehole was drilled to 245 m. It was logged first and then completed with a 4-m slotted casing and a 2-m open section at the bottom. The first borehole tested the Sewickley coal (close to the top of the completion) and its immediate strata below including sandy shale and part of the

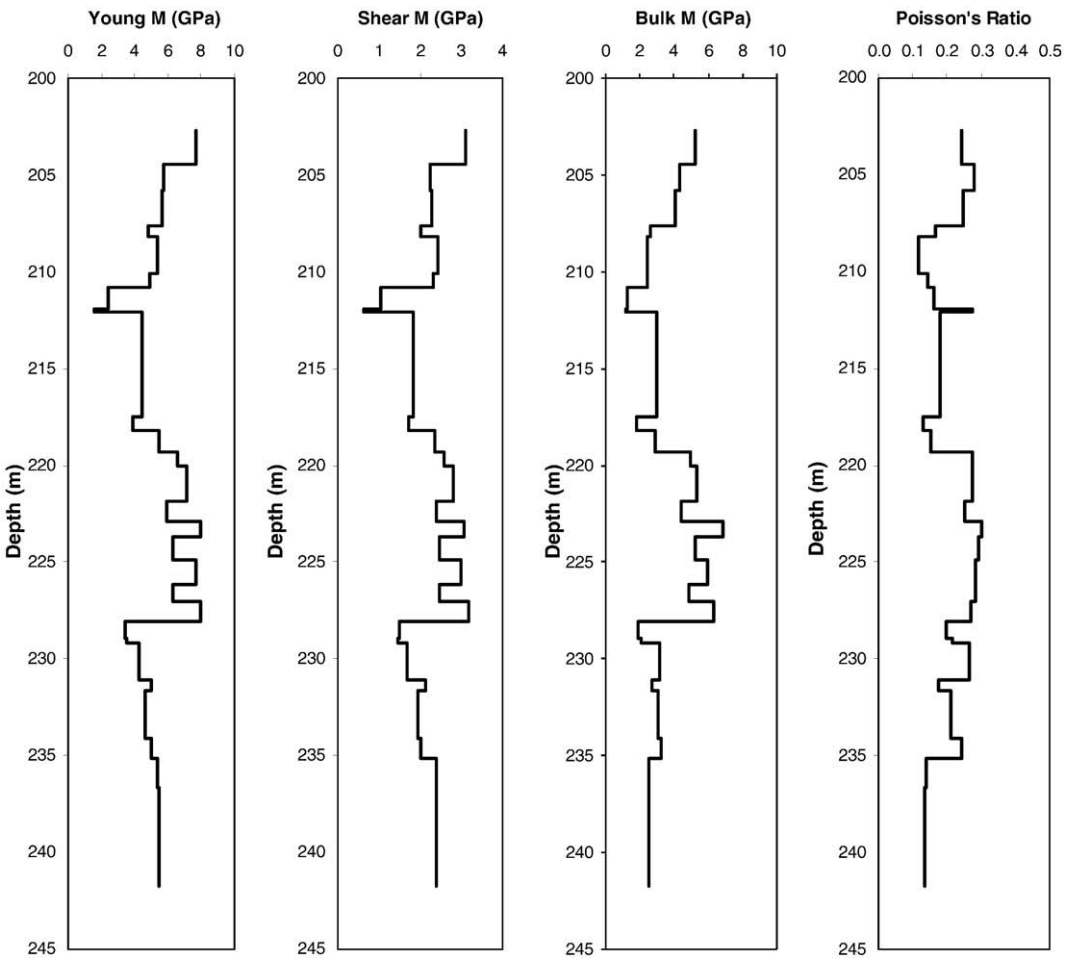

Fig. 13. Young's, shear, and bulk moduli and Poisson's ratio calculated using SL data for EB-2.

limestone. The second borehole tested a majority of the thick limestone layer, and EB-2 tested the Pittsburgh sandstone and overlying sandy shale unit (Fig. 8).

After completing the boreholes by casing and cementing, the boreholes were instrumented with downhole transducers located close to the top of slotted sections to protect them from any sludge that might have been at the bottom of the boreholes. The transducer used in this test was a self-contained data logger and pressure transducer with a 2.041 MPa (300 psia) rating. The data stored in the transducer could be uploaded to a computer at the surface through this cable using the accompanying software. After installing and starting the transducers, the boreholes were filled with water as quickly as possible to start the slug tests. The data were recorded and initially downloaded in 15-second intervals, followed by 30-minute intervals later in the tests. The tests took approximately 1 week in each borehole.

The data obtained from the slug tests were analyzed using the Bauwer and Rice (1976) method that is also summarized in Dawson and Istok (1991). The average permeabilities calculated for the tested intervals were 2.8 md, 0.11 md, and 0.14 md for the first, second, and third test borehole (EB-2), respectively. These values are actually close to the permeabilities obtained from the laboratory tests (Table 6). This suggests that the slug tests measured permeabilities mainly in the fracture-free sections of the formations and thus close to the matrix permeability values.

5.3.2. Permeability calculations using empirical models with well log data

Two models were used to calculate the permeability of different rock layers using log data. These models were those of Timur (1968) and the empirical equation proposed by Yan (2002) for a shaly sand reservoir in the North Sea.

Shale content and porosity are believed to control permeability in clay-sand formations (Yan, 2002). According to core analysis of permeability, porosity, and shale content determination in the laboratory and calibrating these data with log responses, Yan proposed the following empirical equation for permeability of shaly-sand formations:

$$k = a\times 10^4 \frac{\phi_{\log}^b}{V_{sh}^c} \tag{9}$$

where a, b, and c are coefficients which were determined by non-linear regression (Yan, 2002) and their values are 8.71, 5.78 and 1.37, respectively. In this equation, Φ is the porosity calculated from density or neutron logs, V_{sh} is the shale content, which can be calculated from the gamma ray log, and k is permeability. Since shale content is included in this equation, porosity can be used without correcting it for shale volume effects.

The Timur model is based on the work of Wyllie and Rose (1950). This model is given in Balan et al. (1995) for permeability calculation:

$$k = 0.136\frac{\phi_{\log}^{4.4}}{S_{wi}^2}. \tag{10}$$

In this equation, S_{wi} is irreducible water saturation. In our calculation, we have assumed that S_{wi}=S_w and that the formations

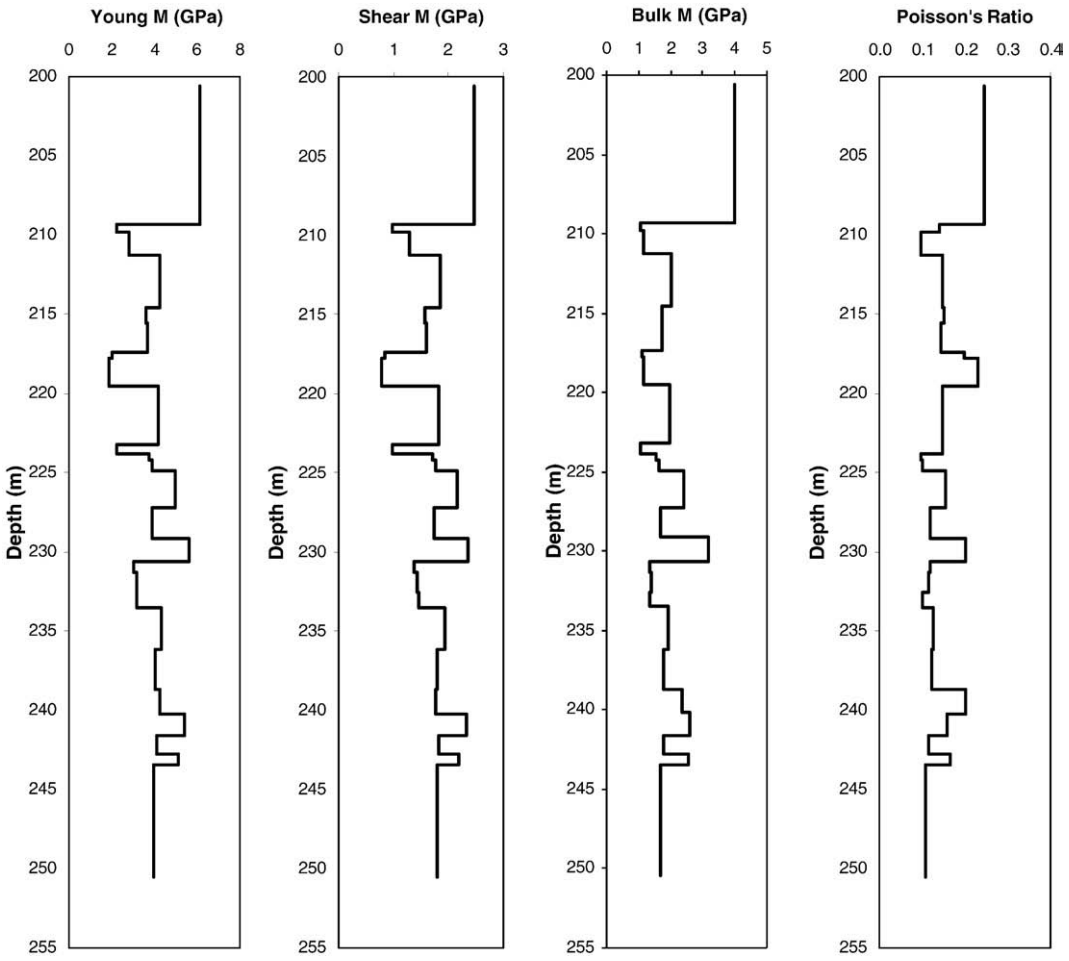

Fig. 14. Young's, shear, and bulk moduli and Poisson's ratio calculated for EB-1 using fractal techniques and radial basis functions on gamma and density logs (Karacan, 2008).

around the boreholes were 100% saturated with water. Considering the fact that the boreholes were drilled with water and logging was performed as soon as drilling was completed, this assumption is reasonable.

Fig. 16-A and B shows permeability values calculated with Eqs. (9) and (10), respectively, for the entire interval of the EB-2 borehole. These values show that the permeabilities are generally low except for some particular intervals. These intervals correspond to the "weak" intervals at the strata interfaces or "suspected fractures" within the formations discussed in the previous sections. The high values in those layers are on the order of 1100–9000 md at 212 m and 90 md at 229 m in the Fig. 16-A log that was generated using Yan's (2002) formula. The

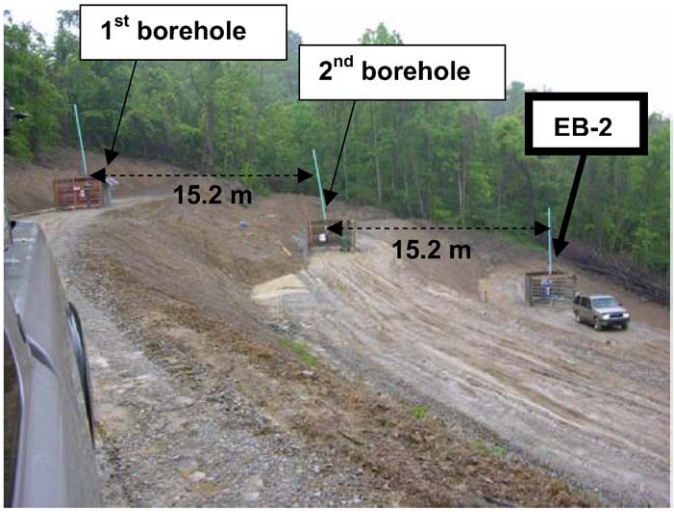

Fig. 15. Test site where slug tests were performed in the boreholes (A) and the downhole transducer used to collect data during tests.

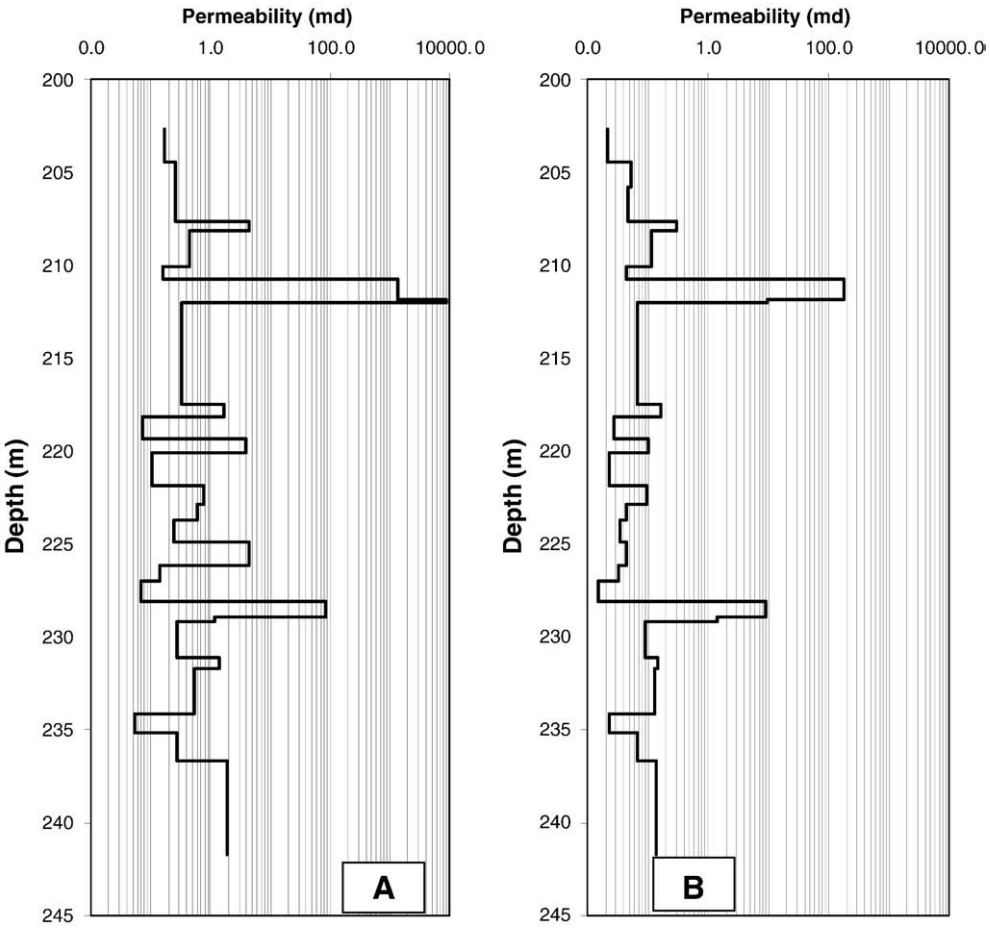

Fig. 16. Permeability logs for EB-2 borehole generated using Yan (2002) equation (A), and Timur (1968) equation (B).

same locations have 180 md and 9 md in Fig. 16-B, calculated using Timur's (1968) formula. The other intervals have low permeabilities on the order of 0–3 md, with an average of 1.16 md, in Fig. 16-A and 0–0.3 md, with an average of 0.18 md, as shown in Fig. 16-B. As seen from the calculated permeabilities, the difference between these two methods is almost one order of magnitude and may result from the different parameters used in these equations. However, it is not unusual for empirical models to give somewhat different values (Balan et al., 1995). Except for two high-permeability intervals, all permeabilities are very low and the predictions from both models can be considered close to each other for the ranges reported. They also can be considered in good agreement with laboratory and with slug test measurements given in previous sections.

Fig. 17-A and B shows permeability values calculated for the EB-1 borehole for the entire interval using its logs and Eqs. (9) and (10). Similarly to EB-2, there are also high-permeability layers at this location at depths of 210 m (40 md), 218 m (680 md) and 244 m (35 md) in Fig. 17-A. The rest of the rock layers have lower permeabilities between 0 and 2 md. The average of low-permeability layers is 0.6 md. For permeability logs calculated using the Timur equation (Fig. 17-B), one interval at 224 m has the highest permeability layer of 22 md. Other higher-permeability intervals are 7.5 and 14 md at depths of 210 and 218 meters, respectively. Low permeability intervals have an average permeability value of 0.4 md. These values are in good agreement with each other and with the results of laboratory and slug testing.

6. Summary and concluding remarks

The methane emission rate into an underground mine environment from overburden strata during longwall mining is impacted by reservoir and geomechanical characteristics of the coal measure rocks in the overlying strata, as well as the presence of any coal seam. The reservoir characteristics and how they change during mining potentially affect the performance of gob gas ventholes, which consequently impacts the efficiency of methane control in the mining environment.

This paper presents a preliminary reservoir and mechanical characterization of coal measure formations in the Lower Monongahela Group from exploration boreholes drilled in Greene County, Southwestern Pennsylvania, using laboratory analyses and gamma ray, density, and sonic logs.

Core porosities and permeabilities were determined and log analyses of formation boundaries, in-situ porosities, existing fractures, and geomechanical properties (shear, Young's, and bulk moduli and Poisson's ratio) were reported. Permeabilities were determined using slug tests in the boreholes and were compared with the permeabilities calculated using two empirical equations. The results of this paper can serve as a source of basic properties for coal measure rocks and can be used for gob gas venthole designs and for constructing models for reservoir and geomechanical simulations.

Specific observations and conclusions can be stated as:

1. In the Lower Monongahela Group of coal measure formations, most of the strata are composed of shale-rich sequences with occasional thick limestone and sandstone layers. Cores recovered from a borehole showed that layers are mostly fine-grained sediments, without much primary porosity and permeability. However, there are natural fractures within the interval, especially in the bedding plane interfaces, which may help drain pockets of gas and water before mining occurs.
2. Laboratory analyses of core plugs drilled from cores showed that primary porosities are within 1–2% in most rock types, except with some higher numbers between 5 and 10% depending on the rock

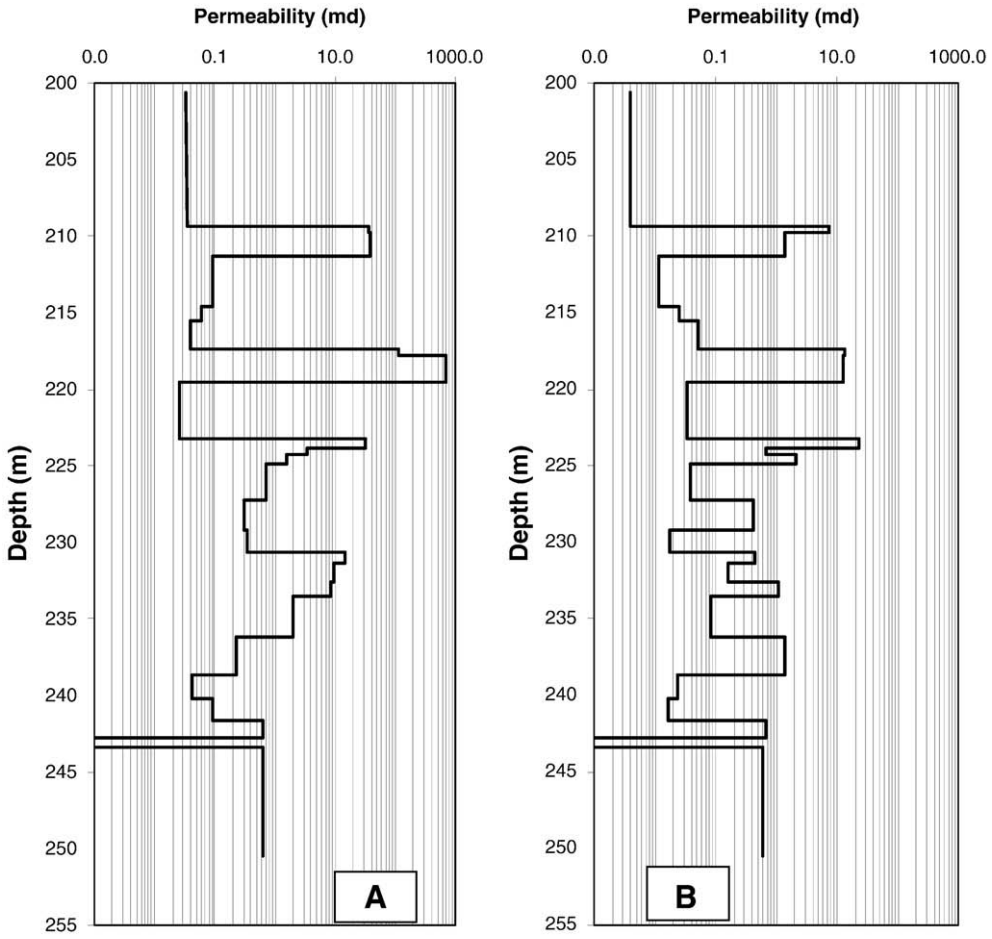

Fig. 17. Permeability logs for EB-1 borehole generated using Yan (2002), equation (A), and Timur (1968), equation (B).

type and the existence of micro cracks in the matrices. Measured matrix permeabilities are generally less than 1 md. However, values increasing to 2–6 md were measured depending on the existence of fissures in the matrices.

3. Wellbore logs that are commonly used in the petroleum and natural gas industry can be used in the mining industry for purposes other than determining the thicknesses of the coal and the immediate roof material. Well logs can be used more effectively in the coal mining industry for characterizing the reservoir and mechanical properties of the entire coal measure strata that will stay in the fractured interval during mining. These logs can be used to determine shale content, porosity, elastic moduli of rocks, Poisson's ratio, fractured intervals or intervals amenable for fracturing, and permeability. This information can help optimize the location and design of GGVs to capture methane more effectively.
4. Gamma ray and density logs were used to determine shale contents and porosities of the Monongahela Group. These logs showed that there are possible fracturing and separation zones between hard- and soft-rock interfaces. The existence of fractures within the single rock units was also observed. The porosities without shale correction were calculated at 5–10%. However, considering the shaliness of formations and their effects on density log readings, a correction was applied on the porosity data. Shale content for most intervals was around 40%, except for lower values in thick limestone intervals. Corrected porosity values were 10–15%.
5. Sonic log data was used to calculate the secondary porosity index which defined the fractured intervals and their porosities.
6. Full wave sonic log and wave velocities were used to calculate Young's, shear and bulk moduli of the entire interval. Young's and bulk moduli varied from 4 to 8 GPa, depending on the rock type. Shear moduli showed lower values. The strongest formation was determined to be the limestone interval with the coal and pure shales being the weakest. Poisson's ratio values were 0.15–0.25 for the entire interval.
7. Permeabilities of coal measure rocks were calculated using log data and empirical equations. The values calculated with two different equations were close and they were also in close agreement with the laboratory-measured permeabilities and with data from the slug tests. Higher permeability values were calculated for “possible” fractures, which could not be tested at the laboratory and were also missed in slug-tested intervals. Thus, log data can be used to estimate the permeability of fractures in the formation.

Acknowledgements

Drs. Ilkin Bilgesu of West Virginia University and Ronald McDowell of the West Virginia Geological and Economic Survey are acknowledged for their help in laboratory analysis of cores. Drs. Robert McLendon and Duane Smith of DOE-NETL in Morgantown are acknowledged for making X-ray CT available for this study. The operating mine in Greene County is also acknowledged for giving permission to have the borehole cores analyzed.

References

Advanced Logic Technologies, 2008. WellCAD v. 4.2. Luxenbourg.
Balan, B., Mohaghegh, S., Ameri, S., 1995. State-of-the-Art in permeability determination from well log data: part 1 — a comparative study, model development. SPE Paper no: 30978, Proceedings of SPE Eastern Regional Meeting, Morgantown, WV.

Bauwer, H., Rice, R.C., 1976. A slug test for determining hydraulic conductivity of unconfined aquifers with completely or partially penetrating wells. Water Resources Research 12, 423–428.
Beamish, B.B., Crosdale, P.J., 1998. Instantaneous outbursts in underground coal mines: an overview and association with coal type. International Journal of Coal Geology 35, 27–55.
Bemer, E., Vincke, O., Longuemare, P., 2004. Geomechanical log deduced from porosity and mineralogical content. Oil and Gas Science and Technology 59, 405–426 – Rev. IFP.
Castagna, J.P., Batzle, M.L., Eastwood, R.L., 1985. Relationships between compressional-wave and shear-wave velocities in clastic silicate rocks. Geophysics 4, 571–581.
Dawson, K.J., Istok, J.D., 1991. Aquifer testing: design and analysis of pumping and slug tests. Lewis Publishers, MI.
Deisman, N., Gentzis, T., Chalaturnyk, R.J., 2008. Unconventional geomechanical testing on coal for coalbed reservoir well design: the Alberta Foothills and Plains. International Journal of Coal Geology 75, 15–26.
Diamond, W.P., Bodden, W.R., Zuber, M.D., Schraufnagel, R.A., 1989. Measuring the extent of coalbed gas drainage after 10 years of production at the Oak Grove Pattern, Alabama. Paper 8961, Proc. Coalbed Methane Symposium, Tuscaloosa, AL.
Dresser Atlas. 1974. Log Review I. Dresser Atlas Division, Dresser Industries.
Endo, T., 2006. Evaluation of formation permeability from borehole Stoneley waves. Journal of Geography 115, 883–899.
Hatherly, P., Medhurst, T., Sliwa, R., Turner, R., 2005. A rock mass assessment procedure based on quantitative geophysical log analysis of coal measure sequences. Exploration Geophysics 36, 112–117.
Karacan, C.Ö. 2008. Elastic and shear moduli of coal measure rocks derived from basic well logs using fractal statistics (fGn/fBm) and radial basis function (RBF) networks. *Submitted to International Journal Rock Mechanics and Mining Sciences*.
Karacan, C.Ö., Mitchell, G.D., 2003. Behavior and effect of coal microlithotypes during gas transport for carbon dioxide sequestration into coal seams. International Journal of Coal Geology 53, 201–217.
Karacan, C.Ö., Esterhuizen, G.S., Schatzel, S.J., Diamond, W.P., 2007. Reservoir simulation-based modeling for characterizing longwall methane emissions and gob gas venthole production. International Journal of Coal Geology 71, 225–245.
Kelafant, J.R., Wicks, D.E., Kuuskraa, V.A., 1988. A geologic assessment of natural gas from coal seams of the Northern Appalachian basin. Topical Report GRI 88/0039, Gas Research Institute, Chicago, IL. 86 pp.
Ketcham, R.A., Carlson, W.D., 2001. Acquisition, optimization and interpretation of X-ray computed tomographic imagery: applications to the geosciences. Computers and Geosciences 27, 381–400.
King, G.R., Ertekin, T., 1994. A survey of mathematical models related to methane production from coal seam: III. Recent developments (1989–1993). The International Coalbed Methane Extraction Conference, London, UK.
King, G.R., Ertekin, T., Schwerer, F.C., 1986. Numerical simulation of the transient behavior of coal-seam degasification wells. Society of Petroleum Engineers (SPE) Formation Evaluation, pp. 165–183. April.
Lunarzewski, W.L., 1998. Gas emission prediction and recovery in underground coal mines. International Journal of Coal Geology 35, 117–145.
Lyons, A., 1998. The central and northern Appalachian Bain — a frontier region for coalbed methane development. International Journal of Coal Geology 38, 61–87.
Markowski, A., 1998. Coalbed methane resource potential and current prospect in Pennsylvania. International Journal of Coal Geology 38, 137–159.
Milkereit, B., Ji, J., 2005. Extraction of Stoneley waves from full wave sonic data. Proceedings of EAGE 67th Conference and Exhibition, Madrid, Spain.
Noack, K., 1998. Control of gas emissions in underground coal mines. International Journal of Coal Geology, 35, 57–82.
Norris, A., 1989. Stoneley-wave attenuation and dispersion in permeable formations. Geophysics 54, 330–341.
Palchik, V., 2003. Formation of fractured zones in overburden due to longwall mining. Environmental Geology 44, 28–38.
Palchik, V., 2005. Localization of mining-induced horizontal fractures along rock layer interfaces in overburden: field measurements and prediction. Environmental Geology 48, 68–80.
Penn State University Libraries, 2000. Description of the geology of Greene County Pennsylvania. URL: http://www.libraries.psu.edu/emsl/guides/X/greene.htm.
Qobi, A., Kuijper, A., Ting, X.M., Strauss, J., 2001. Permeability determination from Stoneley waves in the Ara Group carbonates, Oman. GeoArabia 6, 649–666.
Remner, D.J., Ertekin, T., Sung, W., King, G.R., 1986. A parametric study of the effects of coal seam properties on gas drainage efficiency. SPE Reservoir Engineering 633–645 November.
Ruppert, L.F., Tewalt, S.J., Bragg, L.J., Wallack, R.N., 1999. A digital resource model of the Upper Pennsylvanian Pittsburgh coal bed, Monongahela Group, northern Appalachian Basin coal region, USA. International Journal of Coal Geology 41, 3–24.
Schlumberger, 1991. Log Interpretation Principles/Applications. Schlumberger Wireline and Testing, Sugarland, TX.
Silitonga, T.H., Siahaan, E.E., 2005. A Poisson's ratio distribution from Wadati diagram as indicator of fracturing of Lahendong geothermal field, North Sulawesi, Indonesia. Proceedings of World Geothermal Congress, Antalya, Turkey.
Takahashi, T., Takeuchi, T., Sassa, K., 2006. ISRM suggested methods for borehole geophysics in rock engineering. International Journal of Rock Mechanics and Mining Sciences 43, 337–368.
Timur, A., 1968. An investigation of permeability, porosity and residual water saturation relationships for sandstone reservoirs. The Log Analyst 9, 30–48.
Vaziri, H.H., Wang, X., Palmer, I.D., Khodaverdian, M., McLennan, J., 1997. International Journal of Rock Mechanics and Mining Sciences 34, 963–978.
Whittles, D.N., Lowndes, I.S., Kingman, S.W., Yates, C., Jobling, S., 2006. Influence of geotechnical factors on gas flow experienced in a UK longwall coal mine panel. International Journal of Rock Mechanics and Mining Sciences 43, 369–387.
Whittles, D.N., Lowndes, I.S., Kingman, S.W., Yates, C., Jobling, S., 2007. The stability of methane capture boreholes around a longwall coal panel. International Journal of Coal Geology 71, 313–328.
Wyllie, M.R.J., Rose, W.D., 1950. Some theoretical considerations related to the quantitative evaluation of the physical characteristics of reservoir rock from electric log data. Trans AIME 189, 105.
Yan, J., 2002. Reservoir parameters estimation from well log and core data: a case study from the North Sea. Petroleum Geoscience 8, 63–69.